iScience

CellPress

Article

Conjugated Polymers with Oligoethylene Glycol Side Chains for Improved Photocatalytic Hydrogen Evolution

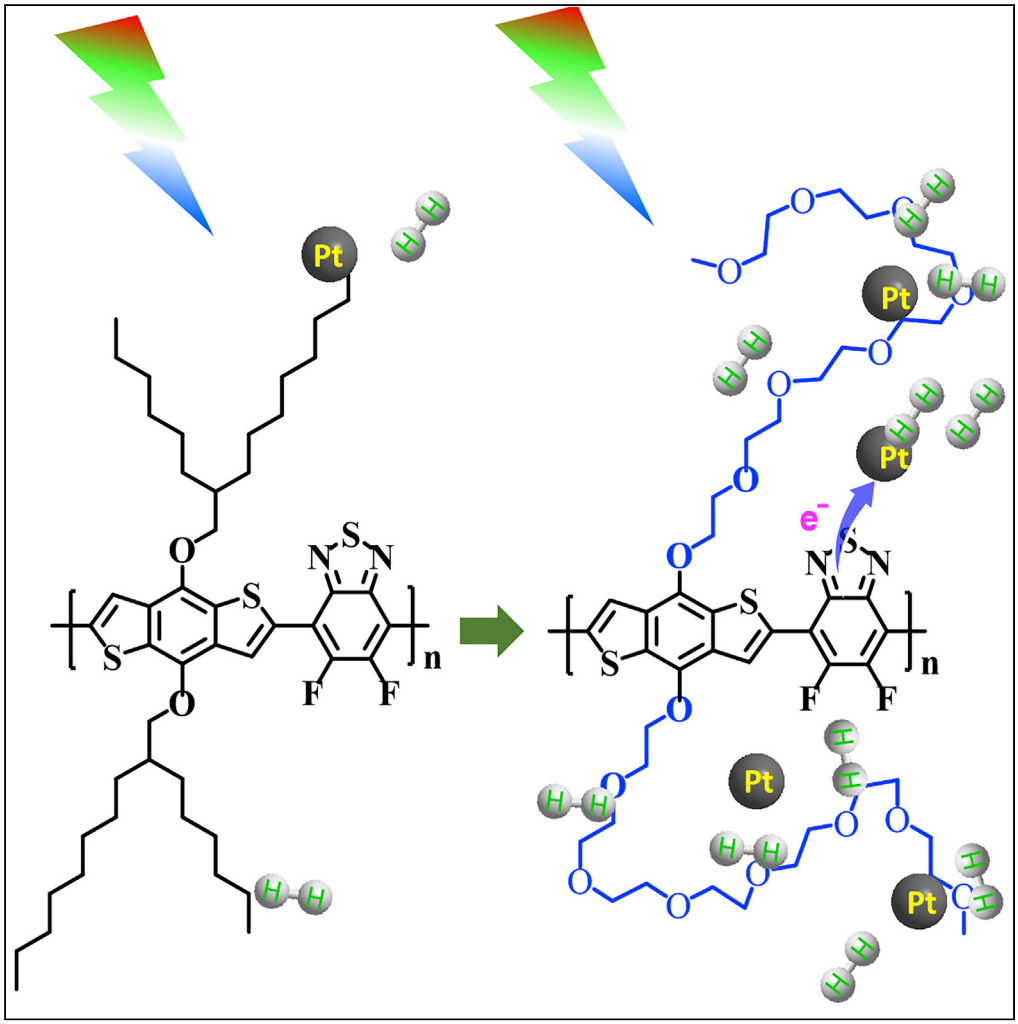

Zhicheng Hu, Zhenfeng Wang, Xi Zhang, Haoran Tang, Xiaocheng Liu, Fei Huang, Yong Cao

msfhuang@scut.edu.cn

HIGHLIGHTS

Conjugated polymers with oligoethylene glycol side chains are prepared

Oligoethylene glycol side chains improve photocatalytic hydrogen evolution rates

Oligoethylene glycol side chains interact robustly with Pt co-catalysts

Oligoethylene glycol side chains enable cascade energy levels

Hu et al., iScience 13, 33–42
March 29, 2019
https://doi.org/10.1016/j.isci.2019.02.007

iScience

CellPress

Article

Conjugated Polymers with Oligoethylene Glycol Side Chains for Improved Photocatalytic Hydrogen Evolution

Zhicheng Hu,[1,2] Zhenfeng Wang,[1] Xi Zhang,[1] Haoran Tang,[1] Xiaocheng Liu,[1] Fei Huang,[1,2,3,*] and Yong Cao[1]

SUMMARY

Conjugated polymers are emerging as promising organic photocatalysts for hydrogen evolution from water. However, it is still very challenging for conjugated polymers to realize highly efficient photocatalytic hydrogen evolution. Herein, we demonstrate an efficient strategy of hydrophilic side chain functionalization to boost the hydrogen evolution rates of conjugated polymers. By functionalizing conjugated polymers with hydrophilic oligo (ethylene glycol) monomethyl ether (OEG) side chains, a 90-fold improvement in hydrogen evolution rate has been achieved than that of alkyl-functionalized conjugated polymer. It is found that the OEG side chains interact robustly with Pt co-catalysts, resulting in more efficient charge transfer. Moreover, OEG side chains in conjugated polymers can adsorb H^+ from water, resulting in significantly lowered energy levels on the surfaces of conjugated polymers, which enables cascade energy levels and enhances charge separation and photocatalytic performance. Our results indicate that rational side-chain engineering could facilitate the design of improved organic photocatalysts for hydrogen evolution.

INTRODUCTION

Photocatalytic hydrogen evolution from water is a promising technology to transfer solar energy into hydrogen energy with high-energy capacity and zero-emission features. Since the pioneering research of Honda and Fujishima, there has been much work on the development of semiconductors that enable efficient photocatalytic water splitting (Fujishima and Honda, 1972; Chen et al., 2017a; Ding et al., 2016; Ong et al., 2016). Organic photocatalysts for photocatalytic hydrogen evolution have received tremendous attention in the past several years (Ong et al., 2016; Vyas et al., 2016; Zhang et al., 2016; Fu et al., 2018; Wang et al., 2018a, 2018b; Yang et al., 2018; Lan et al., 2018; Ou et al., 2018) because of their unique feature of tunable electronic properties via molecular engineering (Zhang et al., 2017). The energy levels, absorption spectrum, and carrier mobility/type of organic photocatalysts can be easily tuned to realize efficient water reduction/oxidation. Consequently, various polymers with tailor-made chemical structures have been extensively studied. For example, g-C_3N_4 (Wang et al., 2009; Martin et al., 2014; Lau et al., 2016), porous conjugated polymers(Sprick et al., 2015; Li et al., 2016a; Yang et al., 2016; Wang et al., 2017), covalent conjugated polymers (Vyas et al., 2015; Pachfule et al., 2018), and linear conjugated polymers (Sprick et al., 2016; Li et al., 2016b; Lu et al., 2017; Woods et al., 2017; Pati et al., 2017; Tseng et al., 2018; Kosco et al., 2018) have been widely developed as organic photocatalysts for hydrogen evolution and have shown promising photocatalytic activity over the past few years. Moreover, through multiple modification strategies, including doping (Liu et al., 2010; Ran et al., 2015), hybridization (Du et al., 2012; Chen et al., 2017b; Yu et al., 2018), and copolymerization (Zhang et al., 2010) on organic photocatalysts, highly efficient hydrogen evolution can be realized. In addition, suitable metal co-catalysts have been used to lower the redox overpotential and improve charge transfer and separation, which has greatly improved the photocatalytic performance of organic photocatalysts (Wu et al., 2018).

To achieve high-performance hydrogen evolution, it is required that organic photocatalysts with strong light-harvesting capabilities and suitable energy levels be designed (Ong et al., 2016; Vyas et al., 2016; Zhang et al., 2016; Fu et al., 2018; Wang et al., 2018c; Yang et al., 2018). Furthermore, because of the short exciton diffusion length (Peumans et al., 2004) and low mobility of organic materials, the powder size of organic photocatalysts dispersed in water must be small to provide shorter distances for the separated charges emigrating to the edges of the organic photocatalysts, thus reducing the recombination inside the organic photocatalysts. Moreover, strong interactions between organic photocatalysts and

[1]Institute of Polymer Optoelectronic Materials and Devices, State Key Laboratory of Luminescent Materials and Devices, South China University of Technology, Guangzhou 510640, P. R. China

[2]South China Institute of Collaborative Innovation, Dongguan 523808, PR China

[3]Lead Contact

*Correspondence: msfhuang@scut.edu.cn

https://doi.org/10.1016/j.isci.2019.02.007

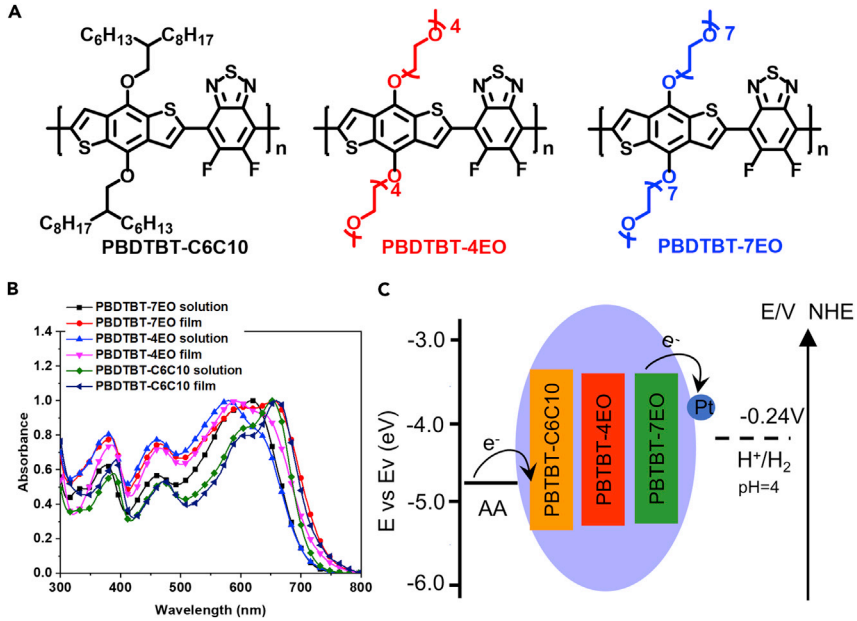

Figure 1. Chemical Structures and Basic Properties of Conjugated Polymers

(A) Chemical structures of PBDTBT-C6C10, PBDTBT-4EO, and PBDTBT-7EO.

(B) UV-vis-NIR absorption spectra of PBDTBT-C6C10, PBDTBT-4EO, and PBDTBT-7EO.

(C) Energy levels of conjugated polymers and the energy transfers among photocatalysts, co-catalysts, scarifying agent, and water.

metal co-catalysts are also encouraged to improve charge separation (Lau et al., 2016). However, it is challenging to realize all these characteristics because most reported organic materials/conjugated polymer-based photocatalysts sharing hydrophobic alkyl side chains show poor water dispersion (Li et al., 2016b) and lack binding points with metal co-catalysts.

Hydrophilic conjugated polymers share both semiconductive conjugated backbones and hydrophilic side chains (Duan et al., 2013; Chueh et al., 2015; Cui and Bazan, 2018). The hydrophilic side chains impart polymers with excellent dispersity/solubility in polar solvents and water, enabling the application of such polymers in biosensing and imaging applications (Traina et al., 2011). Moreover, hydrophilic side chains can robustly interact with metal substrates, resulting in well-modified metal surfaces that promote optoelectronic device performance (Duan et al., 2013; Chueh et al., 2015; Cui and Bazan, 2018). The advantages of hydrophilic conjugated polymers are identical to the requirements of organic photocatalysts for hydrogen evolution. However, despite the above-mentioned multiple potential advantages, hydrophilic conjugated polymers for highly efficient hydrogen evolution have rarely been reported.

Herein, we demonstrate a highly efficient strategy to boost the photocatalytic hydrogen evolution of conjugated polymers by functionalizing conjugated backbones with hydrophilic oligo (ethylene glycol) monomethyl ether (OEG) side chains. With rational chemical design, benzodithiophene and difluorobenzothiadiazole moieties were copolymerized to yield conjugated polymeric backbones with a wide absorption spectrum of 300–720 nm. Moreover, hydrophilic tetra- and hepta-(ethylene glycol) monomethyl ether side chains were employed to modify the conjugated polymer backbones (PBDTBT-4EO/PBDTBT-7EO, Figure 1A), resulting in outstanding dispersion of conjugated polymers in water and high photocatalytic activity for hydrogen evolution. Compared with an alkyl-functionalized polymer (PBDTBT-C6C10, Figure 1A), the OEG side-chain-functionalized conjugated polymers exhibited a 90-fold improvement in hydrogen evolution rate, reaching to 40 μmol h^{-1}. The OEG side chains interact robustly with Pt co-catalysts, resulting in better charge transfer from the conjugated polymers to the co-catalysts. The photocurrent response and electrochemical impedance spectroscopy results showed that OEG side chains improved the charge separation efficiency of the conjugated polymers when in contact with water. The Mott–Schottky plots and density functional theory (DFT) calculations revealed that the OEG side chains in conjugated polymers can adsorb H^+ in water, resulting in lower energy bands of PBDTBT-4EO/-7EO

film on the surface when in contact with water. This is the first report of conjugated polymers with hydrophilic side chains strongly interacting with water and improving charge separation, which paves the way for the development of hydrophilic conjugated polymers for highly efficient hydrogen evolution from water.

RESULTS AND DISCUSSION

Conjugated polymers with OEG side chains (PBDTBT-4EO and PBDTBT-7EO, Figure 1A) were synthesized using Stille polymerization from OEG-functionalized benzodithiophene monomers and difluorobenzothiadiazole monomer (BT). For comparison, PBDTBT-C6C10 (Figure 1A) with alkyl side chains was also prepared. The synthetic details of these polymers can be found in the Transparent Methods section in Supplemental Information, and the chemical structures of these conjugated polymers were confirmed by ^{1}H NMR, ^{13}C NMR (Figure S1), and Fourier transform infrared spectroscopy (Figure S2). The average molecular weights of PBDTBT-C6C10, PBDTBT-4EO, and PBDTBT-7EO were estimated to be 20.1, 26.4, and 29.6 kDa, respectively. The poly(benzodithiophene-alt-difluorobenzthiadiazole) (PBDTBT) backbones possess multiple advantages for hydrogen evolution. First, the PBDTBT backbones show wide absorption spectra covering the visible range, which may drive efficient hydrogen evolution in visible light. Second, the nitrogen atoms in the BT units present a low hydrogen binding free energy (ΔG_H) of about 0.632 eV (Figure S3), indicating the potential high-performance photocatalytic hydrogen evolution of PBDTBT (Pati et al., 2017). The side chain alternation on the conjugated polymers could further endow these polymers with different properties. Compared with PBDTBT-C6C10, which possesses hydrophobic side chains, PBDTBT-4EO and PBDTBT-7EO with OEG side chains exhibit much better dispersity in water because of the hydrogen bonding between the OEG side chains and water (Traina et al., 2011).

The absorption spectra of these conjugated polymers were investigated using UV-vis absorption spectroscopy. As shown in Figure 1B, the absorption spectra of PBDTBT-C6C10, PBDTBT-4EO, and PBDTBT-7EO cover the absorption range from 300 to 720 nm, implying excellent utilization of sunlight, especially in the visible range. PBDTBT-7EO exhibits a slightly broadened thin-film absorption spectrum in the wavelength from 680 to 750 nm than that of PBDTBT-C6C10, implying the formation of larger aggregation and better crystallinity (Chang et al., 2014), which can be evidenced by their X-ray powder diffraction (XRD) results (Figure S4). The optical band gaps of these polymers were calculated to be 1.71, 1.72, and 1.72 eV, respectively. The energy levels of these polymers were investigated using cyclic voltammetry analysis, and the results are presented in Figures 1C and S5. The highest occupied molecular orbit (HOMO) and lowest unoccupied molecular orbital (LUMO) energy levels of PBDTBT-C6C10 were calculated to be −5.41 and −3.36 eV, respectively. The HOMO energy levels of PBDTBT-4EO and PBDTBT-7EO were slightly up-shifted to about −5.29 and −5.27 eV, respectively, which can be attributed to the electron-donating effect of the OEG side chains. The LUMO energy levels were calculated to be −3.38 and −3.39 eV, respectively, similar to the level in PBDTBT-C6C10.

To examine the hydrophilic properties of PBDTBT-4EO/-7EO, we tested the water contact angles of these polymers as thin films. The water contact angles of PBDTBT-C6C10, PBDTBT-4EO, and PBDTBT-7EO were 101.2°, 33.9°, and 27.5°, respectively (Figure S6), indicating that the OEG side chains can effectively improve the hydrophilic properties of conjugated polymers. It has been shown that improved wettability of conjugated polymers will lead to better dispersity of conjugated polymers and better photocatalytic performance (Vyas et al., 2016). The much-reduced water contact angles of PBDTBT-4EO and PBDTBT-7EO indicates that the hydrophilic OEG side chains resulted in better interface wettability with water and balanced the short exciton diffusion length of the conjugated polymers by providing shorter paths for separated charges emigrating to the edges of the polymers, which is highly desirable for hydrogen evolution.

The transmission electron microscopy (TEM) images (Figures 2A–2C) of the dispersed conjugated polymers in water showed that these polymers can be dispersed well in water forming small-sized nanoparticles. Compared with PBDTBT-C6C10, which form small aggregates with average size and distribution of 24.1 ± 5.1 nm (Figure S7), PBDTBT-4EO and PBDTBT-7EO can form even smaller aggregates in water. Especially, PBDTBT-7EO showed the smallest aggregates and best dispersity in water with average size and distribution of 5.9 ± 1.1 nm (Figure S7). The much smaller size of PBDTBT-7EO aggregates will provide much more surface area for co-catalysts loading and shorter distances for the separated charges emigrating to the edges of the organic photocatalysts, both of which are highly desired for improving

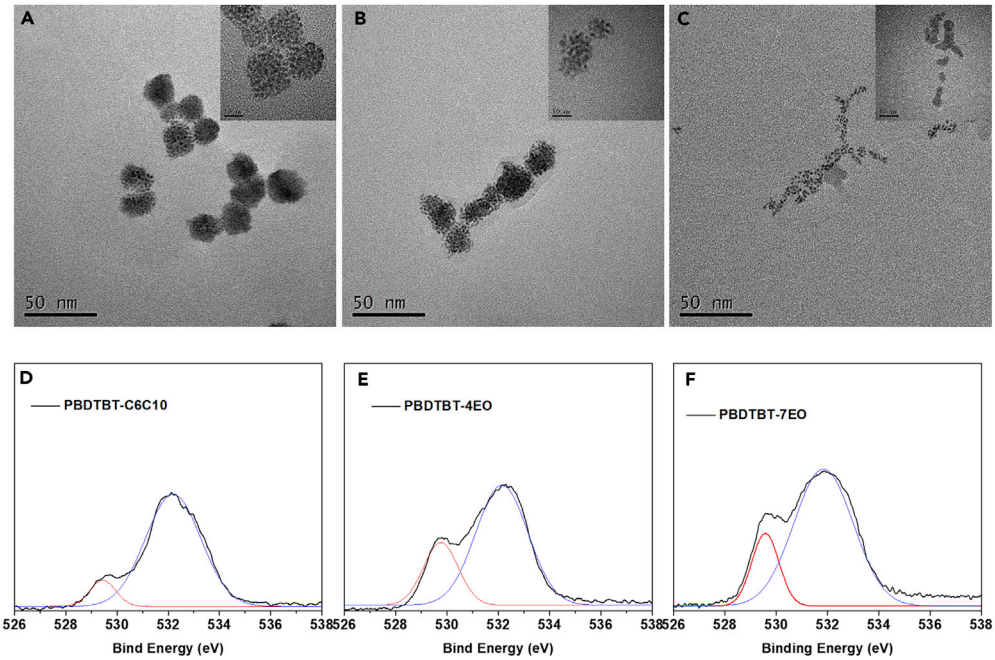

Figure 2. TEM Images and XPS O1s Spectra

(A–C) TEM images of PBDTBT-C6C10 (A), PBDTBT-4EO (B), and PBDTBT-7EO (C) dispersed in water (the scale bar in insets represents 10 nm).

(D–F) XPS O1s spectra for PBDTBT-C6C10 (D), PBDTBT-4EO (E), and PBDTBT-7EO (F) films upon Pt sheets.

photocatalytic hydrogen evolution. The XRD analysis (Figure S4) of conjugated polymer powders indicates that the OEG functionalized polymers possess a π-π stacking distance closer than that of PBDTBT-C6C10. The closer stacking distance of OEG functionalized polymers could facilitate charge transporting along the conjugated backbones, which can reduce the charge recombination inside polymers and potentially improve photocatalytic activity.

X-ray photoelectron spectroscopy (XPS) was used to analyze the interaction between these polymers and Pt co-catalysts. We used thin Pt sheets instead of Pt nanoparticles, upon which thin layers of conjugated polymers (~3 nm) were spin coated. It can be observed that a weak O1s peak corresponding to the O–Pt interaction at 529.6 eV (Rajumon et al., 1998) occurred in PBDTBT-C6C10 (Figure 2D). However, this signal became much more pronounced in PBDTBT-4EO and PBDTBT-7EO films (Figures 2E and 2F), indicating much stronger interactions between PBDTBT-4EO/-7EO and the Pt sheets. Thus, it can be easily deduced that the OEG side chains provide more intimate contact between conjugated polymers and Pt co-catalysts, resulting in better charge transfer (Li et al., 2017).

The photocatalytic hydrogen evolution of these polymers was evaluated using ascorbic acid (AA) as a scarifying agent and Pt (3 wt% of the polymers) as co-catalyst. These polymers were dispersed in water and ultrasonicated for 1 h before testing. The volumes of generated hydrogen as a function of time are presented in Figures 3A and 3B. It can be observed that hydrogen production increases linearly with increasing time. The hydrogen evolution rate (HER) of PBDTBT-C6C10 was calculated to be 0.45 μmol h^{-1} from the plot of produced H_2 as a function of time. Surprisingly, PBDTBT-4EO with OEG side chains showed enhanced photocatalytic performance with a HER of 18.03 μmol h^{-1}. The much-improved photocatalytic performance in PBDTBT-4EO indicates that the side chains of conjugated polymers play a key role in the photocatalytic process. Moreover, the HER of PBDTBT-7EO was further enhanced to 39.75 μmol h^{-1} compared with that of PBDTBT-4EO (a 90-fold enhancement), indicating that the longer hydrophilic side chains enable higher utilization of the conjugated polymers and higher photocatalytic activity. For comparison, PBDTBT without side chains were also prepared and tested. PBDTBT showed a lower HER of 5.2 μmol h^{-1} (Figure S8), which is much lower than that of PBDTBT-4EO and PBDTBT-7EO. Note that this performance is among the best of conjugated polymer-based photocatalysts (Tables S1 and S2).

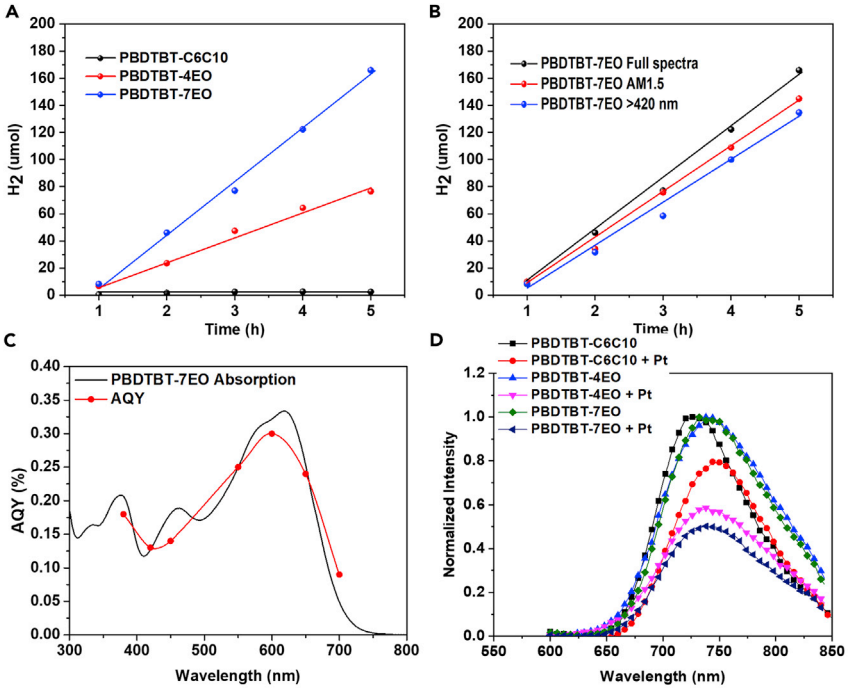

Figure 3. Photocatalytic Performance of Conjugated Polymers

(A) Hydrogen evolution rates of the conjugated polymers with full spectra irradiation.

(B) Hydrogen evolution rates of PBDTBT-7EO at full, >420 nm, and AM1.5 irradiation (reaction conditions: 2.5 mg of polymer dispersed in 50 mL of deionized water containing 0.2 M AA, pH = 4.0).

(C) Absorption spectrum of PBDTBT-7EO and apparent quantum yield (AQY) values as a function of light wavelength.

(D) Photoluminescence emission spectra of PBDTBT-C6C10, PBDTBT-4EO, and PBDTBT-7EO with/without Pt co-catalysts.

The photocatalytic activities of PBDTBT-7EO in different spectra were also investigated (Figure 3B). With an AM1.5 spectrum illumination, a HER of 34.5 μmol h^{-1} was obtained, whereas a HER of 32.0 μmol h^{-1} was achieved for testing with a 420-nm filter cut-off. The apparent quantum yield (AQY) as a function of light wavelength was also collected. As shown in Figure 3C, at 380, 420, 450, 550, 600, 650, and 700 nm, PBDTBT-7EO rendered AQY values of 0.18%, 0.13%, 0.14%, 0.25%, 0.30%, 0.24%, and 0.09%, respectively, indicating a broad photoresponse of PBDTBT-7EO for photocatalysis. The photocatalytic stability of OEG functionalized conjugated polymers was also tested (Figures S9 and S10). With illumination over 44 h (seven runs), PBDTBT-4EO delivered a HER of around 16.4 μmol h^{-1}, which is 90% of the initial HER of PBDTBT-4EO (Figure S9).

Photoluminescence (PL) spectra of these polymers as thin films with/without Pt co-catalysts were obtained to investigate the charge transfer efficiency between conjugated polymer and Pt co-catalysts. It has been reported that modifying the energy communication between photocatalysts and co-catalysts can enhance the charge transfer from photocatalysts to co-catalysts and improve the photocatalytic performance (Li et al., 2017). In our case, the OEG side chains efficiently enhanced the interaction between the conjugated polymers and the Pt co-catalysts, resulting in improved charge transfer and better photocatalytic performance. As shown in Figure 3D, the PL spectra of these polymers were apparently quenched. For PBDTBT-4EO and PBDTBT-7EO, the PL quenching efficiency was higher than that of PBDTBT-C6C10 with Pt co-catalysts, indicating more efficient charge transfer from PBDTBT-4EO/-7EO to the Pt co-catalysts.

The photocurrent responses of these polymers as thin films were measured to further explore their electronic properties. The polymers were coated onto indium tin oxide electrodes and tested with no voltage or −0.2 V applied. As shown in Figure 4A, with no voltage applied, the PBDTBT-4EO/PBDTBT-7EO films showed apparently enhanced (about five times) current density responses compared with the

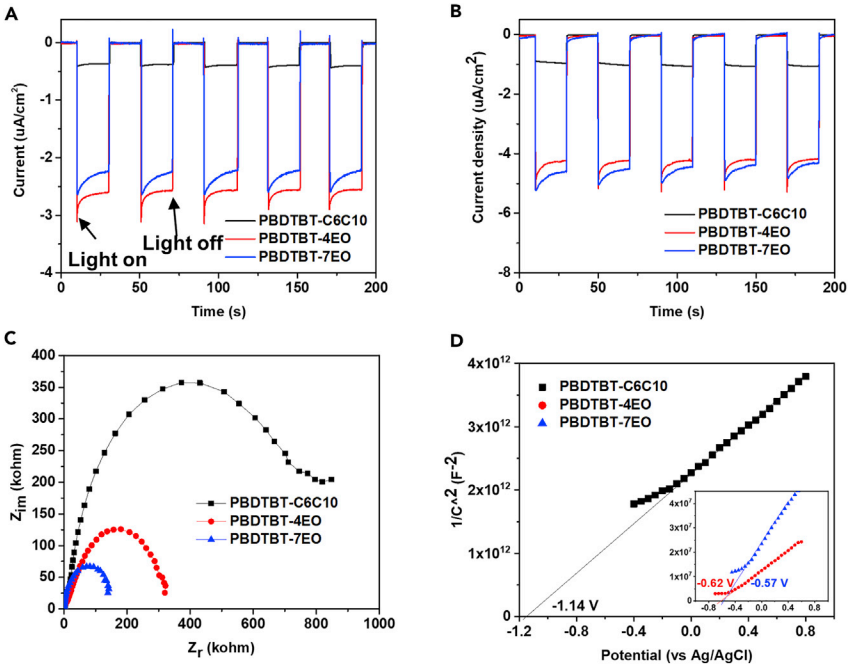

Figure 4. Photocurrent Response, EIS Nyquist Plots, and Mott–Schottky Plots

(A and B) Photocurrent response of the conjugated polymers at applied voltages of 0 V (A) and −0.2 V (B) (with 0.1 M Na_2SO_4 as the electrolyte).

(C) EIS Nyquist plots of conjugated polymers in the dark.

(D) Mott–Schottky plots of PBDTBT-C6C10, PDBDTBT-4EO, and PBDTBT-7EO.

PBDTBT-C6C10 film. A similar phenomenon was observed when −0.2 V (vs. Ag/AgCl) was applied to these films (Figure 4B), indicating that photo-excited charge carriers inside PBDTBT-4EO/-7EO are more strongly promoted than those in PBDTBT-C6C10 (Wang et al., 2018c). Electrochemical impedance spectroscopy (EIS) was also performed, and the semicircular Nyquist plots of these polymers are shown in Figure 4C. The Nyquist plot diameters of PBDTBT-4EO/-7EO are much less than that of PBDTBT-C6C10. In particular, the Nyquist plot diameters decreased with increasing length of the OEG side chains, indicating that the OEG side chains greatly improved the charge transfer properties in the polymer/water interface, which is beneficial for improved photo-excited charge separation (Zhang and Wang, 2014; Dutta and Ouyang, 2015).

The Mott–Schottky plots of these polymer films are shown in Figures 4D, S11, and S12. The positive slopes of the linear plots of these polymers imply the n-type characteristics of these polymers. The flat-band potentials (E_{fb}) of these polymers were then determined (details are shown in Supplemental Information) from the linear plots by intercepting with voltage axis. The E_{fb} values of PBDTBT-C6C10, PBDTBT-4EO, and PBDTBT-7EO were derived to be −1.14, −0.62, and −0.57 V vs. Ag/AgCl, respectively, indicating that the E_{fb} values of PBDTBT-4EO/-7EO were much more positive than those of PBDTBT-C6C10, even though these three polymers possess same backbones. It should be noted that the E_{fb} values of PBDTBT-4EO/-7EO were very close to the redox potential of the electrolyte (−0.60 V vs. Ag/AgCl for 0.1 M Na_2SO_4). The obvious change in E_{fb} values in these polymers implied stronger interactions between PBDTBT-4EO/-7EO and water. Generally, E_{fb} indicates the energy band position (approximately equal to the Fermi level [E_F] [Li et al., 2016c]) of the semiconductor regarding to the redox potentials of the electroactive species in the electrolyte. Here, the changed E_{fb} values in the PBDTBT-4EO/-7EO films indicate that the E_F values of PBDTBT-4EO/-7EO down-shifted when in contact with water. Considering that the only difference in these polymers was their side chains, it can be deduced that the OEG side chains and their interaction with water were the determining factors that led to such an E_F shift.

Before studying the interaction between these polymers and water, we first conducted UV photoelectron spectroscopy (UPS) to determine the pristine relative E_F and ionization potentials (IPs) of these polymers.

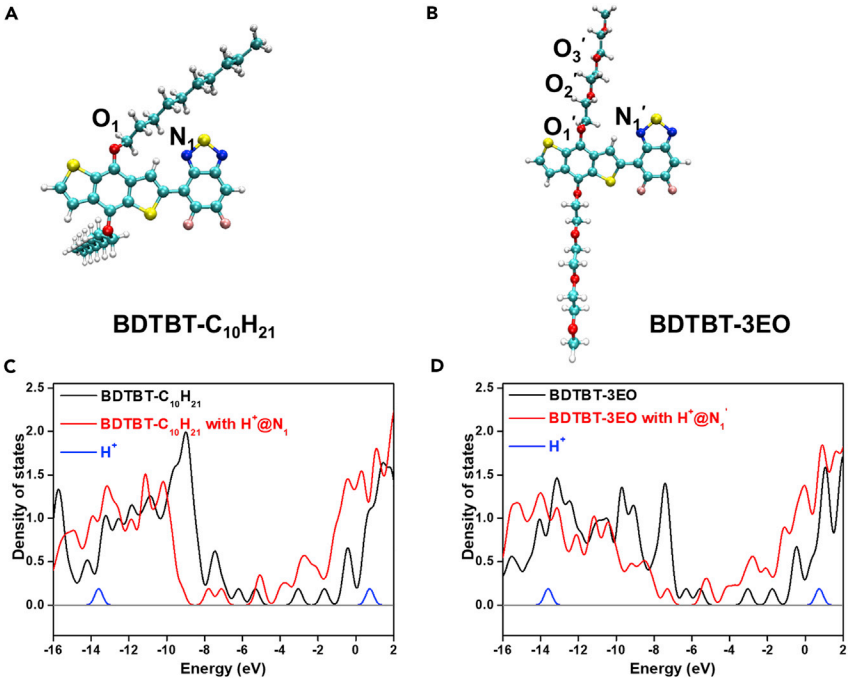

Figure 5. DFT Calculation

(A and B) Optimized geometry of oligomers BDTBT-C10H21 (A) and BDTBT-3EO (B).

(C and D) DOS of BDTBT-$C_{10}H_{21}$ (C) and BDTBT-3EO (D) with H^+ adsorbed at nitrogen sites (the case of one hydrogen atom).

As shown in Figure S13, from the high binding-energy onsets, the E_F values of PBDTBT-C6C10, PBDTBT-4EO, and PBDTBT-7EO were determined to be 3.88, 3.82, and 3.74 eV, respectively. The IPs of PBDTBT-C6C10, PBDTBT-4EO, and PBDTBT-7EO were 5.59, 5.53, and 5.43 eV, determined from their low binding-energy onsets of UPS spectra. The band gaps calculated from IP and E_F are 1.71, 1.71, and 1.69 eV for PBDTBT-C6C10, PBDTBT-4EO, and PBDTBT-7EO, respectively, values that are very close to their band gaps obtained from UV-vis absorption spectra. These results indicated that OEG side chains had a limited effect on the E_F values and energy levels of the pristine conjugated polymers. However, after coming into contact with water, the estimated E_F values in the surfaces of the PBDTBT-4EO and PBDTBT-7EO films down-shifted greatly in comparison with that of the PBDTBT-C6C10 film (Figure S14), approaching the redox potential of the electrolyte. These results indicate that OEG side chains interacted with water more strongly than the -C6C10 side chains. More specifically, the oxygen atom in OEG side chains acted as a medium to improve the interface contact of the conjugated backbones with water, resulting in large changes in the energy levels of the conjugated polymers (Hu et al., 2017).

Heteroatoms in conjugated polymers are regarded as active sites that can interact with proton and catalyze hydrogen evolution reaction (Pati et al., 2017; Pei et al., 2017). To examine the effect of OEG side chains for free H^+ binding, the model oligomers with two -$C_{10}H_{21}$ and tri-(ethylene glycol) monomethyl ether side chains (BDTBT-$C_{10}H_{21}$ and BDTBT-3EO) were submitted for DFT calculations at the level of B3LYP-D3(BJ)/def2-TZVP (Goerigk and Grimme, 2011). The optimized geometries of BDTBT-$C_{10}H_{21}$ and BDTBT-3EO are presented in Figures 5A and 5B. The binding energy between the side chains and H^+ was carefully examined by scanning the contact distance for H^+ at different oxygen sites on the side chains of BDTBT-$C_{10}H_{21}$ and BDTBT-3EO. As shown in Figure S15, the optimized minimum contact distances were around 1 Å, and thus the minimum binding energy was obtained. As shown in Table 1, the minimum binding energy between the O_1 site (in BDTBT-$C_{10}H_{21}$) and H^+ was calculated to be −8.568 eV, whereas those between the O_3', O_2', and O_1' sites (in BDTBT-3EO) and H^+ were calculated to be −8.164, −8.202, and −8.426 eV in gradient, respectively, suggesting that the OEG side chains act more like H^+ transport channels, enabling closer contact between H^+ and the conjugated backbones. Moreover, the minimum binding energies at N_1 and N_1' of the backbone were much lower (−9.531 and −9.500eV) than those at the oxygen site, indicating that the N atoms are potential active sites for final H^+ reduction (Pati et al., 2017). These

		Binding Energy[a] (eV)	LUMO+1 (eV)	LUMO (eV)	HOMO (eV)	HOMO-1 (eV)
BDTBT-$C_{10}H_{21}$			−1.66	−3.04	−5.32	−6.20
	O_1	−8.57	−4.72	−5.59	−8.73	−9.17
	N_1	−9.53	−5.15	−7.10	−7.79	−9.22
BDTBT-3EO			−1.74	−3.03	−5.57	−6.31
	O_3'	−8.16	−4.54	−5.30	−7.11	−7.81
	O_2'	−8.20	−5.02	−5.16	−7.79	−8.13
	O_1'	−8.43	−4.81	−5.60	−8.32	−8.70
	N_1'	−9.50	−5.36	−7.29	−8.03	−8.32

Table 1. Binding Energy between H^+ and Oxygen/Nitrogen Sites in BDTBT-$C_{10}H_{21}$ and BDTBT-3EO, Calculated LUMO and HOMO Energies of BDTBT-$C_{10}H_{21}$ and BDTBT-3EO with Adsorbed H^+ (the Case of One Hydrogen Atom)

[a]The minimum binding energy between H^+ and O/N sites in BDTBT-$C_{10}H_{21}$ and BDTBT-3EO.

results indicate that the OEG side chains provide many more adsorption sites for H^+ loading, which could potentially accelerate the photocatalytic progress.

To further investigate the effect of H^+ adsorption on the energy levels of these conjugated polymers, we calculated the densities of state (DOS) of BDTBT-$C_{10}H_{21}$ and BDTBT-3EO with H^+ adsorbed at the oxygen and nitrogen sites. As shown in Figures 5C, 5D, and S16, the calculated DOS indicate that the total energy levels can be efficiently lowered, with H^+ adsorbed both in oxygen and nitrogen sites. For BDTBT-$C_{10}H_{21}$, the calculated LUMO and HOMO decreased from −3.04 and −5.32 eV to −7.10 and −7.79 eV, respectively, when the H^+ adsorbed in N_1. Similar observations were found for BDTBT-3EO. Surprisingly, BDT-3EO with adsorbed H^+ in the OEG chains also showed lower total energy levels (with smaller magnitudes, Table 1), indicating that the adsorbed H^+ can significantly lower the energy levels of conjugated polymers.

The much-lowered energy levels of the conjugated polymers with adsorbed H^+ is consistent with the observation of the E_{fb} changes in PBDTBT-4EO/-7EO. In PBDTBT-C6C10, the hydrophobic alkyl side chain hindered the transport of H^+ approaching the conjugated backbones, leading to a negligible energy level shift in PBDTBT-C6C10 films when in contact with water (Figure S17). However, in PBDTBT-4EO/7EO, the hydrophilic OEG side chains can adsorb H^+, resulting in intimate contact between H^+ and the conjugated backbones and apparently down-shifted energy levels (Figure S17). The lowered energy bands on the surface of PBDTBT-4EO/-7EO led to a cascade energy distribution inside PBDTBT-4EO/-7EO, significantly improving charge separation, as also demonstrated by the photocurrent and EIS results. The improved charge separation thus promotes photocatalytic performance of PBDTBT-4EO/-7EO successfully.

In summary, we have presented hydrophilic side-chain-functionalized conjugated polymers for successful application as organic photocatalysts for hydrogen evolution. The OEG side-chain-functionalized conjugated polymers can render a 90-fold improvement in photocatalytic performance over that of alkyl-functionalized conjugated polymers. The OEG side chains interacted robustly with the Pt co-catalysts, resulting in better charge transfer from the polymer to the Pt co-catalysts. Moreover, our findings indicate that the OEG side chains can adsorb H^+ in water, resulting in lowered Fermi level of PBDTBT-4EO/-7EO in the surface in contact with water, which was evidenced by down-shifted E_{fb} of PBDTBT-4EO/-7EO in the polymer/water interface. As a result, the OEG-functionalized conjugated polymers showed improved charge transfer and separation efficiency and resulted in a much higher photocatalytic performance. Our results show that rational side chain engineering can significantly improve the photocatalytic performance of conjugated polymers, facilitating the novel design of organic photocatalysts with highly efficient hydrogen evolution.

METHODS

All methods can be found in the accompanying Transparent Methods supplemental file.

Limitations of Study

In our study, the longer OEG side chains of conjugated polymer enable better dispersion in water and improve the photocatalytic activity. We believe that further optimizing the length of OEG side chains may further enhance the photocatalytic activity of conjugated polymers. However, the relationships between the length of OEG side chains and the HER performance have not been fully studied. More investigation on the optimization of side chains is needed to further improve the HER of conjugated polymers.

SUPPLEMENTAL INFORMATION

Supplemental Information includes Transparent Methods, 17 figures, and 2 tables and can be found with this article online at https://doi.org/10.1016/j.isci.2019.02.007.

ACKNOWLEDGMENTS

This work was financially supported by the Natural Science Foundation of China (No. 21634004, and 21490573) and the Foundation of Guangzhou Science and Technology Project (No. 201707020019). Z.H. thanks the support from the China Postdoctoral Science Foundation (No. 2017M622684).

AUTHOR CONTRIBUTIONS

Z.H., F.H., and Y.C. developed the idea, designed the experiments, and drafted the manuscript. Z.H. synthesized the polymers and performed the photocatalytic experiments. Z.W. and H.T. performed the DFT calculation. X.Z., and X.L. performed the polymer characterization. All the members discussed the results and analyzed the data.

DECLARATION OF INTERESTS

The authors declare no competing interests.

Received: November 9, 2018
Revised: January 22, 2019
Accepted: February 5, 2019
Published: March 29, 2019

REFERENCES

Chang, W.-H., Gao, J., Dou, L., Chen, C.-C., Liu, Y., and Yang, Y. (2014). Side-chain tunability via triple component random copolymerization for better photovoltaic polymers. Adv. Energy Mater. *4*, 1300864.

Chen, S., Takata, T., and Domen, K. (2017a). Particulate photocatalysts for overall water splitting. Nat. Rev. Mater. *2*, 17050.

Chen, J., Dong, C.L., Zhao, D., Huang, Y.C., Wang, X., Samad, L., Dang, L., Shearer, M., Shen, S., and Guo, L. (2017b). Molecular design of polymer heterojunctions for efficient solar–hydrogen conversion. Adv. Mater. *29*, 1606198.

Chueh, C.-C., Li, C.-Z., and Jen, A.K.-Y. (2015). Recent progress and perspective in solution-processed Interfacial materials for efficient and stable polymer and organometal perovskite solar cells. Energy Environ. Sci. *8*, 1160–1189.

Cui, Q., and Bazan, G.C. (2018). Narrow band gap conjugated polyelectrolytes. Acc. Chem. Res. *51*, 202–211.

Ding, C., Shi, J., Wang, Z., and Li, C. (2016). Photoelectrocatalytic water splitting: significance of cocatalysts, electrolyte, and interfaces. ACS Catal. *7*, 675–688.

Du, A., Sanvito, S., Li, Z., Wang, D., Jiao, Y., Liao, T., Sun, Q., Ng, Y.H., Zhu, Z., Amal, R., and Smith, S.C. (2012). Hybrid graphene and graphitic carbon nitride nanocomposite: gap opening, electron–hole puddle, interfacial charge transfer, and enhanced visible light response. J. Am. Chem. Soc. *134*, 4393–4397.

Duan, C., Zhang, K., Zhong, C., Huang, F., and Cao, Y. (2013). Recent advances in water/alcohol-soluble π-conjugated materials: new materials and growing applications in solar cells. Chem. Soc. Rev. *42*, 9071–9104.

Dutta, A., and Ouyang, J. (2015). Ternary NiAuPt nanoparticles on reduced graphene oxide as catalysts toward the electrochemical oxidation reaction of ethanol. ACS Catal. *5*, 1371–1380.

Fu, J., Yu, J., Jiang, C., and Cheng, B. (2018). g-C_3N_4-based heterostructured photocatalysts. Adv. Energy Mater. *8*, 1701503.

Fujishima, A., and Honda, K. (1972). Electrochemical photolysis of water at a semiconductor electrode. Nature *238*, 37–38.

Goerigk, L., and Grimme, S. (2011). A thorough benchmark of density functional methods for general main group thermochemistry, kinetics, and noncovalent interactions. Phys. Chem. Chem. Phys. *13*, 6670–6688.

Hu, Z., Li, Q., Lei, B., Zhou, Q., Xiang, D., Lyu, Z., Hu, F., Wang, J., Ren, T., Guo, R., et al. (2017). Water-catalyzed oxidation of few-layer black phosphorous in a dark environment. Angew. Chem. Int. Ed. *56*, 9131–9135.

Kosco, J., Sachs, M., Godin, R., Kirkus, M., Francas, L., Bidwell, M., Qureshi, M., Anjum, D., Durrant, J.R., and McCulloch, I. (2018). The effect of residual palladium catalyst contamination on the photocatalytic hydrogen evolution activity of conjugated polymers. Adv. Energy Mater. https://doi.org/10.1002/aenm.201802181.

Lan, Z.-A., Fang, Y., Zhang, Y., and Wang, X. (2018). Photocatalytic oxygen evolution from functional triazine-based polymers with tunable band structure. Angew. Chem. Int. Ed. *57*, 470–474.

Lau, V.W.-H., Moudrakovski, I., Botari, T., Weinberger, S., Mesch, M.B., Duppel, V., Senker, J., Blum, V., and Lotsch, B.V. (2016). Rational design of carbon nitride photocatalysts by identification of cyanamide defects as catalytically relevant sites. Nat. Commun. *7*, 12165.

Li, L., Cai, Z., Wu, Q., Lo, W.Y., Zhang, N., Chen, L.X., and Yu, L. (2016a). Rational design of porous conjugated polymers and roles of residual

palladium for photocatalytic hydrogen production. J. Am. Chem. Soc. *138*, 7681–7686.

Li, L., Hadt, R.G., Yao, S., Lo, W.-Y., Cai, Z., Wu, Q., Pandit, B., Chen, L.X., and Yu, L. (2016b). Photocatalysts based on cobalt-chelating conjugated polymers for hydrogen evolution from water. Chem. Mater. *28*, 5394–5399.

Li, H., Yu, H., Quan, X., Chen, S., and Zhang, Y. (2016c). Self-assembled framework enhances electronic communication of ultrasmall-sized nanoparticles for exceptional solar hydrogen evolution. ACS Appl. Mater. Interfaces *8*, 2111.

Li, X.B., Gao, Y.J., Wang, Y., Zhan, F., Zhang, X.Y., Kong, Q.Y., Zhao, N.J., Guo, Q., Wu, H.L., Li, Z.J., et al. (2017). Self-assembled framework enhances electronic communication of ultrasmall-sized nanoparticles for exceptional solar hydrogen evolution. J. Am. Chem. Soc. *139*, 4789–4796.

Liu, G., Niu, P., Sun, C., Smith, S.C., Chen, Z., Lu, G.Q., and Cheng, H.M. (2010). Unique electronic structure induced high photoreactivity of sulfur-doped graphitic C_3N_4. J. Am. Chem. Soc. *132*, 11642–11648.

Lu, H., Hu, R., Bai, H., Chen, H., Lv, F., Liu, L., Wang, S., and Tian, H. (2017). Efficient conjugated polymer–methyl viologen electron transfer system for controlled photo-driven hydrogen evolution. ACS Appl. Mater. Interfaces *9*, 10355–10359.

Martin, D.J., Reardon, P.J.T., Moniz, S.J.A., and Tang, J. (2014). Visible light-driven pure water splitting by a nature-inspired organic semiconductor-based system. J. Am. Chem. Soc. *136*, 12568–12571.

Ong, W.-J., Tan, L.-L., Ng, Y.H., Yong, S.-T., and Chai, S.-P. (2016). Graphitic carbon nitride (g-C3N4)-based photocatalysts for artificial photosynthesis and environmental remediation: are we a step closer to achieving sustainability? Chem. Rev. *116*, 7159–7329.

Ou, H., Chen, X., Lin, L., Fang, Y., and Wang, X. (2018). Biomimetic donor-acceptor motifs in conjugated polymers for promoting exciton splitting and charge separation. Angew. Chem. Int. Ed. *57*, 8729–8733.

Pachfule, P., Acharjya, A., Roeser, J., Langenhahn, T., Schwarze, M., Schomacker, R., Thomas, A., and Schmidt, J. (2018). Diacetylene functionalized covalent organic framework (COF) for photocatalytic hydrogen generation. J. Am. Chem. Soc. *140*, 1423–1427.

Pati, P.B., Damas, G., Tian, L., Fernandes, D.L.A., Zhang, L., Pehlivan, I.B., Edvinsson, T., Araujo, C.M., and Tian, H. (2017). An experimental and theoretical study of an efficient polymer nano-photocatalyst for hydrogen evolution. Energy Environ. Sci. *10*, 1372–1376.

Pei, Z., Gu, J., Wang, Y., Tang, Z., Liu, Z., Huang, Y., Huang, Y., Zhao, J., Chen, Z., and Zhi, C. (2017). Component matters: paving the roadmap toward enhanced electrocatalytic performance of graphitic C_3N_4-based catalysts via atomic tuning. ACS Nano *11*, 6004–6014.

Peumans, P., Yakimov, A., and Forrest, S.R. (2004). Small molecular weight organic thin-film photodetectors and solar cells. J. Appl. Phys. *93*, 3693.

Rajumon, M.K., Roberts, M.W., Wang, F., and Wells, P.B. (1998). Chemisorption of ethanol at Pt(111) and Pt(111)–O surfaces. J. Chem. Soc. Faraday Trans. *94*, 3699–3703.

Ran, J., Ma, T.Y., Gao, G., Du, X.-W., and Qiao, S.Z. (2015). Porous p-doped graphitic carbon nitride nanosheets for synergistically enhanced visible-light photocatalytic H_2 production. Energy Environ. Sci. *8*, 3708–3717.

Sprick, R.S., Jiang, J.X., Bonillo, B., Ren, S., Ratvijitvech, T., Guiglion, P., Zwijnenburg, M.A., Adams, D.J., and Cooper, A.I. (2015). Tunable organic photocatalysts for visible-light-driven hydrogen evolution. J. Am. Chem. Soc. *137*, 3265–3270.

Sprick, R.S., Bonillo, B., Clowes, R., Guiglion, P., Brownbill, N.J., Slater, B.J., Blanc, F., Zwijnenburg, M.A., Adams, D.J., and Cooper, A.I. (2016). Visible-light-driven hydrogen evolution using planarized conjugated polymer photocatalysts. Angew. Chem. Int. Ed. *55*, 1792–1796.

Traina, C.A., Bakus, R.C., II, and Bazan, G.C. (2011). Design and synthesis of monofunctionalized, water-soluble conjugated polymers for biosensing and imaging applications. J. Am. Chem. Soc. *133*, 12600–12607.

Tseng, P.-J., Chang, C.-L., Chan, Y.-H., Ting, L.-Y., Chen, P.-Y., Liao, C.-H., Tsai, M.-L., and Chou, H.-H. (2018). Design and synthesis of cycloplatinated polymer dots as photocatalysts for visible-light-driven hydrogen evolution. ACS Catal. *8*, 7766–7772.

Vyas, V.S., Haase, F., Stegbauer, L., Savasci, G., Podjaski, F., Ochsenfeld, C., and Lotsch, B.V. (2015). A tunable azine covalent organic framework platform for visible light-induced hydrogen generation. Nat. Commun. *6*, 8508.

Vyas, V.S., Lau, V.W.-H., and Lotsch, B.V. (2016). Soft photocatalysis: organic polymers for solar fuel production. Chem. Mater. *28*, 5191–5204.

Wang, X., Maeda, K., Thomas, A., Takanabe, K., Xin, G., Carlsson, J.M., Domen, K., and Antonietti, M. (2009). A metal-free polymeric photocatalyst for hydrogen production from water under visible light. Nat. Mater. *8*, 76–80.

Wang, L., Wan, Y., Ding, Y., Wu, S., Zhang, Y., Zhang, X., Zhang, G., Xiong, Y., Wu, X., Yang, J., and Xu, H. (2017). Conjugated microporous polymer nanosheets for overall water splitting using visible light. Adv. Mater. *29*.

Wang, H., Zhang, X., and Xie, Y. (2018a). Photoresponsive polymeric carbon nitride-based materials: design and application. Mater. Today. https://doi.org/10.1016/j.mattod.2018.05.001.

Wang, L., Zhang, Y., Chen, L., Xu, H., and Xiong, Y. (2018b). 2D Polymers as emerging materials for photocatalytic overall water splitting. Adv. Mater. *30*, 1801955.

Wang, Y., Silveri, F., Bayazit, M.K., Ruan, Q., Li, Y., Xie, J., Catlow, C.R.A., and Tang, J. (2018c). Bandgap engineering of organic semiconductors for highly efficient photocatalytic water splitting. Adv. Energy Mater. *8*, 1801084.

Woods, D.J., Sprick, R.S., Smith, C.L., Cowan, A.J., and Cooper, A.I. (2017). A Solution-processable polymer photocatalyst for hydrogen evolution from water. Adv. Energy Mater. *7*, 1700479.

Wu, H.-L., Li, X.-B., Tung, C.-H., and Wu, L.-Z. (2018). Recent advances in sensitized photocathodes: from molecular dyes to semiconducting quantum dots. Adv. Sci. (Weinh) *5*, 1700684.

Yang, C., Ma, B.C., Zhang, L., Lin, S., Ghasimi, S., Landfester, K., Zhang, K.A.I., and Wang, X. (2016). Molecular engineering of conjugated polybenzothiadiazoles for enhanced hydrogen production by photosynthesis. Angew. Chem. Int. Ed. *55*, 9202–9206.

Yang, C., Huang, W., da Silva, L.C., Zhang, K.A.I., and Wang, X. (2018). Functional conjugated polymers for CO_2 reduction using visible light. Chem. Eur. J. *44*, 17454–17458.

Yu, F., Wang, Z., Zhang, S., Ye, H., Kong, K., Gong, X., Hua, J., and Tian, H. (2018). Molecular engineering of donor–acceptor conjugated polymer/g-c3n4 heterostructures for significantly enhanced hydrogen evolution under visible-light irradiation. Adv. Funct. Mater. https://doi.org/10.1002/adfm.201804512.

Zhang, M., and Wang, X. (2014). Two dimensional conjugated polymers with enhanced optical absorption and charge separation for photocatalytic hydrogen evolution. Energy Environ. Sci. *7*, 1902–1906.

Zhang, J., Chen, X., Takanabe, K., Maeda, K., Domen, K., Epping, J.D., Fu, X., Antonietti, M., and Wang, X. (2010). Synthesis of a carbon nitride structure for visible-light catalysis by copolymerization. Angew. Chem. Int. Ed. *49*, 441–444.

Zhang, G., Lan, Z.A., and Wang, X. (2016). Conjugated polymers: catalysts for photocatalytic hydrogen evolution. Angew. Chem. Int. Ed. *55*, 15712–15727.

Zhang, Q., Kelly, M.A., Bauer, N., and You, W. (2017). The curious case of fluorination of conjugated polymers for solar cells. Acc. Chem. Res. *50*, 2401–2409.

ISCI, Volume *13*

Supplemental Information

Conjugated Polymers with Oligoethylene Glycol Side Chains for Improved Photocatalytic Hydrogen Evolution

Zhicheng Hu, Zhenfeng Wang, Xi Zhang, Haoran Tang, Xiaocheng Liu, Fei Huang, and Yong Cao

Supplemental Information

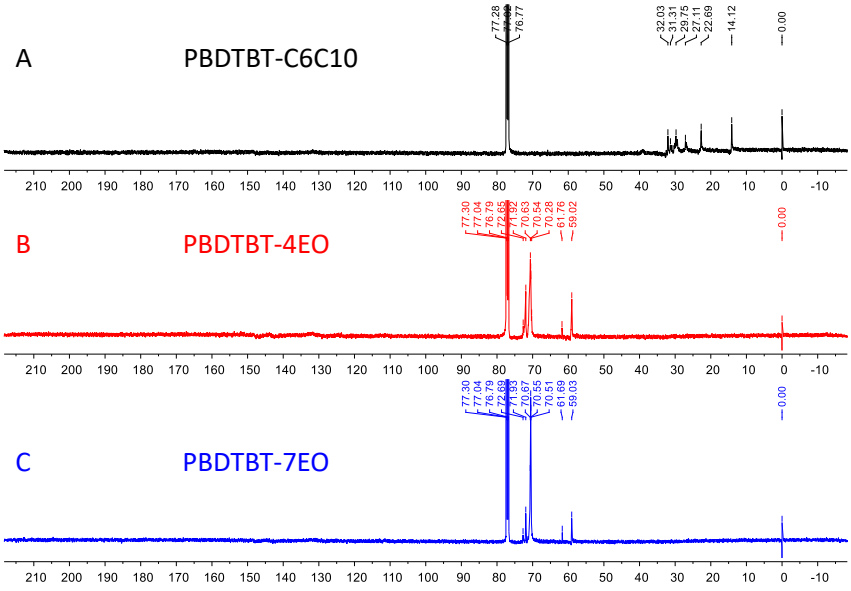

Figure S1. ^{13}C NMR spectra of PBDTBT-C6C10(A), PBDTBT-4EO(B), and PBDTBT-7EO(C) in $CDCl_3$, related to Figure 1. The aromatic carbon signals of these three polymers are difficult to detect due to strong aggregation of these polymer in solvents. The carbon signals of their side chains can be observed, which exhibit chemical shifts of alkyl side chains for PBDTBT-C6C10 and oligoethylene glycol for PBDTBT-4EO and PBDTBT-7EO, respectively.

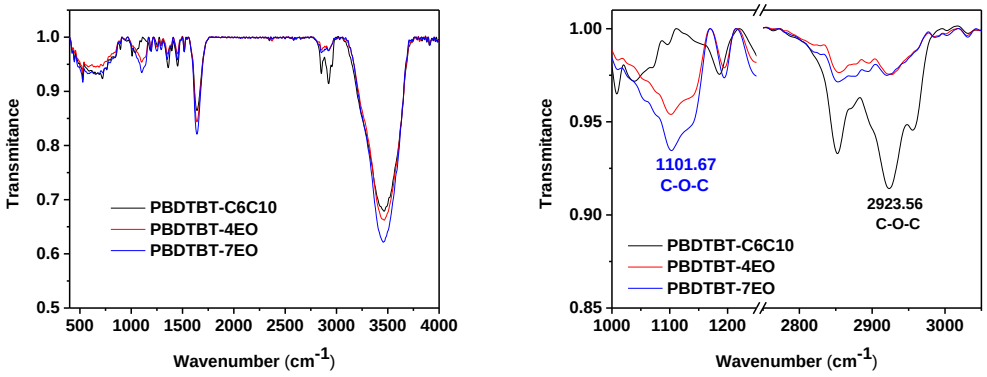

Figure S2. FT-IR spectra of PBDTBT-C6C10, PBDTBT-4EO and PBDTBT-7EO powders, related to Figure 1.

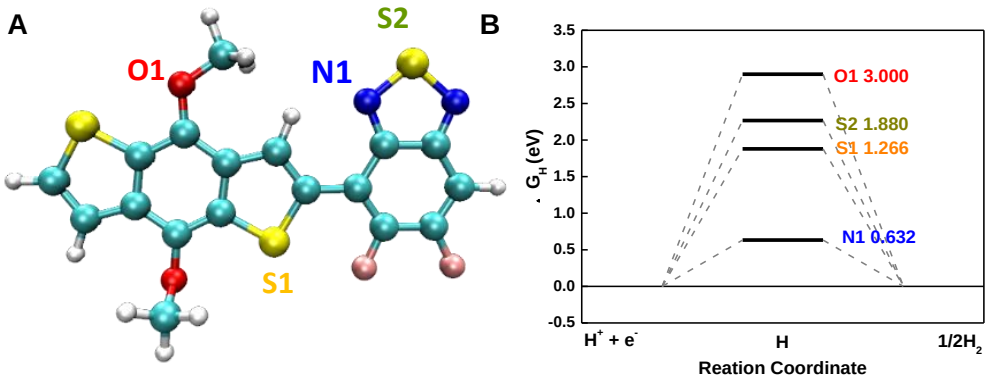

Figure S3. The calculated hydrogen binding free energy (ΔG_H) of heteroatom in backbones of PBDTBT, related to Figure 1. The calculations were performed at the level of B3LYP-D3(BJ)/def2-TZVP.

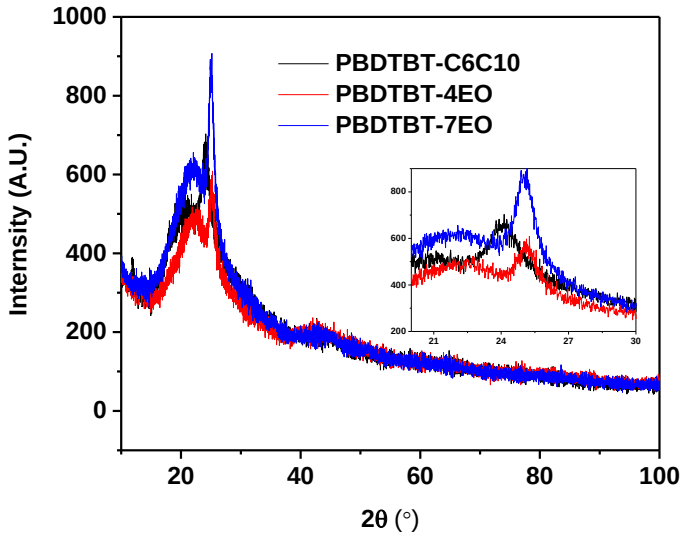

Figure S4. XRD results of conjugated polymers, related to Figure 1. The clear peaks of PBDTBT-C6C10, PBDTBT-4EO and PBDTBT-7EO are located at 24.06°(2θ), 25.11°(2θ)and 24.99°(2θ), corresponding to π–π distances of 3.700 Å, 3.565 Å and 3.548 Å.

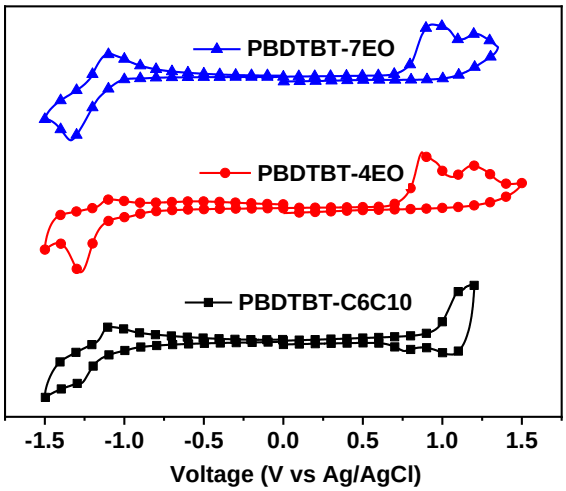

Figure S5. The cyclic voltammetry curves of these polymers, related to Figure 1.

Figure S6. Water contact angles of (A) PBDTBT-C6C10, (B)PBDTBT-4EO, and (C) PBDTBT-7EO films, related to Figure 1.

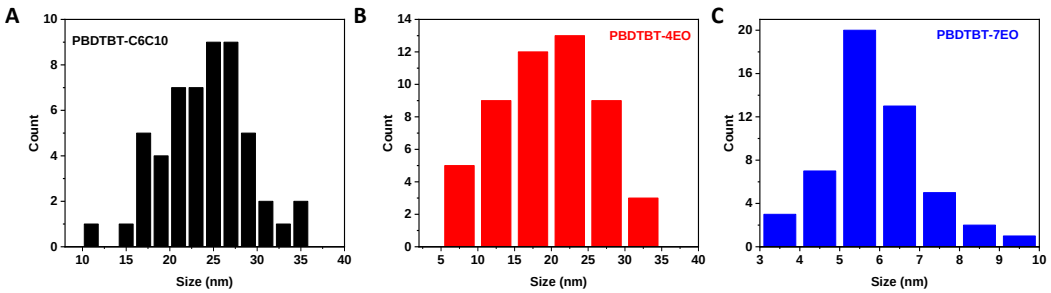

Figure S7. Size distribution of conjugated polymer nanoparticles in water calculated from TEM via image analysis software over 50 nanoparticles, related to Figure 2. PBDTBT-C6C10: 24.1±5.1 nm; PBDTBT-4EO: 19.7±6.5 nm; PBDTBT-7EO: 5.9±1.1 nm.

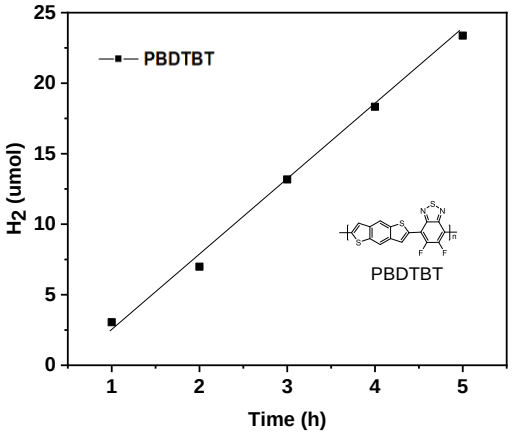

Figure S8. Hydrogen evolution of PBDTBT, related to Figure 3.

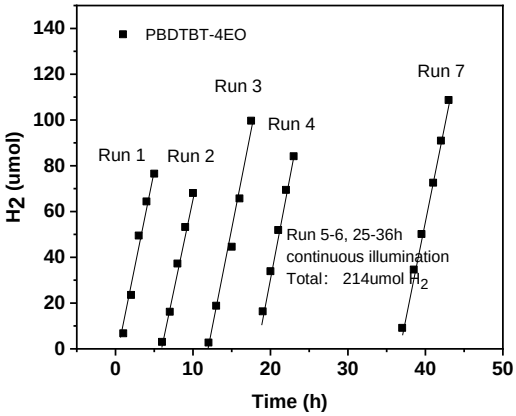

Figure S9. Hydrogen evolution of PBDTBT-4EO with over long-time illumination, related to Figure 3. Average HERs of 18.03 μmolh^{-1} for Run 1, 16.7 μmolh^{-1} for Run 2, 17.07 μmolh^{-1} for Run 3, 17.08 μmolh^{-1} for Run 4, 16.4 μmolh^{-1} for Run 5-6, 16.4 μmolh^{-1} for Run 7.

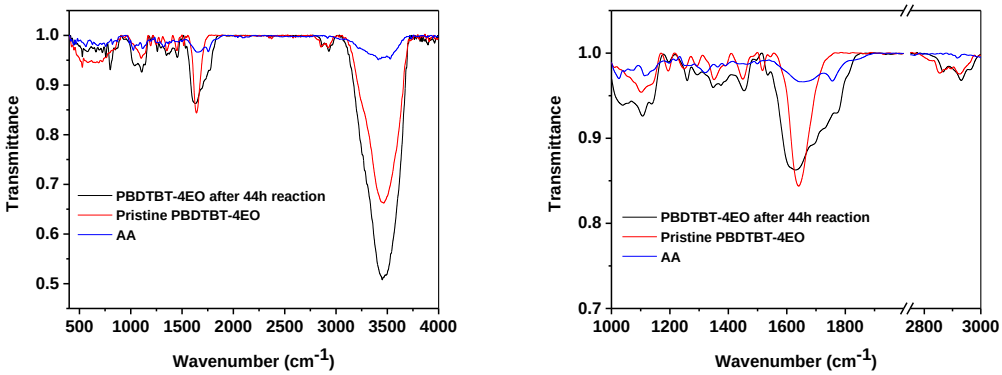

Figure S10. FT-IR spectra of PBDTBT-4EO before and after 44h reaction, related to Figure

3. The FT-IR spectrum of PBDTBT-4EO after reaction is a mixture of the spectra from AA and PBDTBT-4EO, indicating that chemical structure of PBDTBT-4EO 44h reaction is stable.

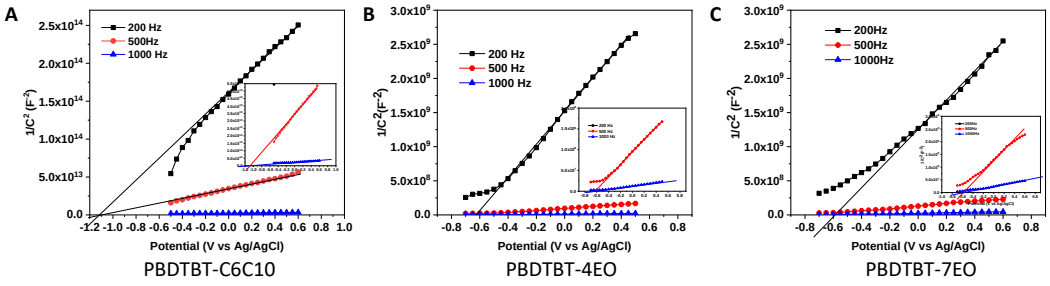

Figure S11. Mott–Schottky plots of PBDTBT-C6C10, PDBDTBT-4EO, and PBDTBT-7EO in 200Hz, 500Hz and 1000Hz, related to Figure 4.

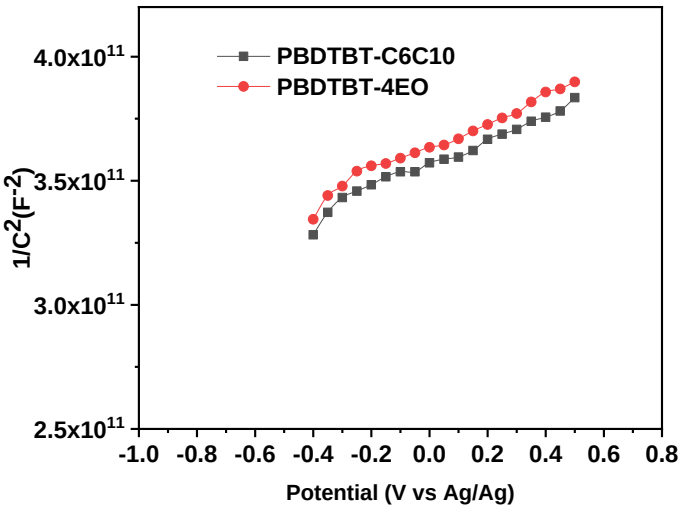

Figure S12. Mott–Schottky plots of PBDTBT-C6C10, and PDBDTBT-4EO in in anhydrous acetonitrile, related to Figure 4.

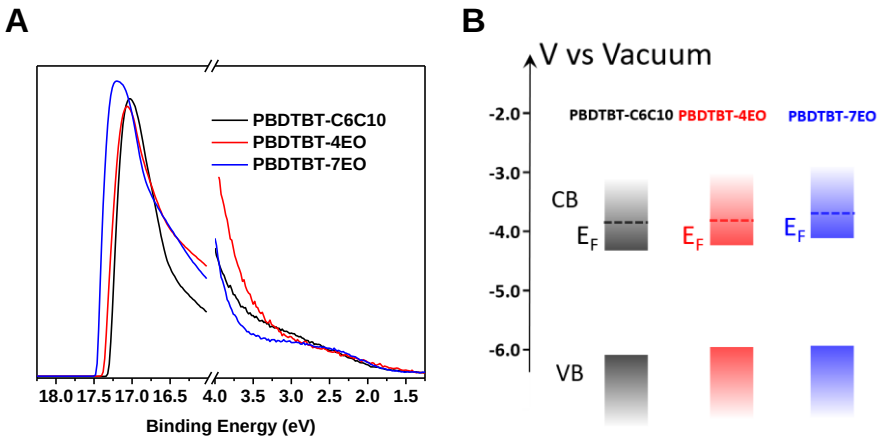

Figure S13. (A) UPS spectra and (B) energy band positions of PBDTBT-C6C10, PBDTBT-4EO, and PBDTBT-7EO, related to Figure 4.

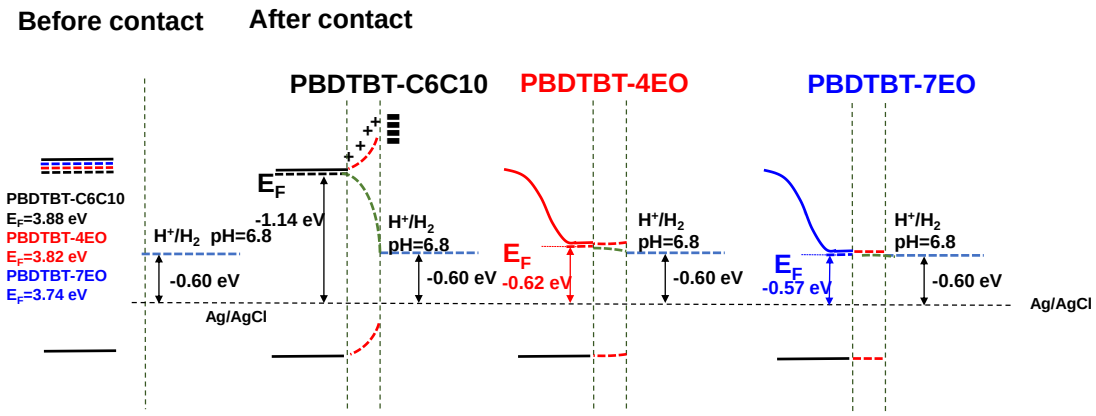

Figure S14. The fermi levels of PBDTBT-C6C10, PBDTBT-4EO and PBDTBT-7EO in the state of before and after contacting with water, related to Figure 4. The fermi levels before contact were determined by UPS, while the fermi levels after contact were determined approximately by E_{FB} referred to the redox potential of electrolyte.

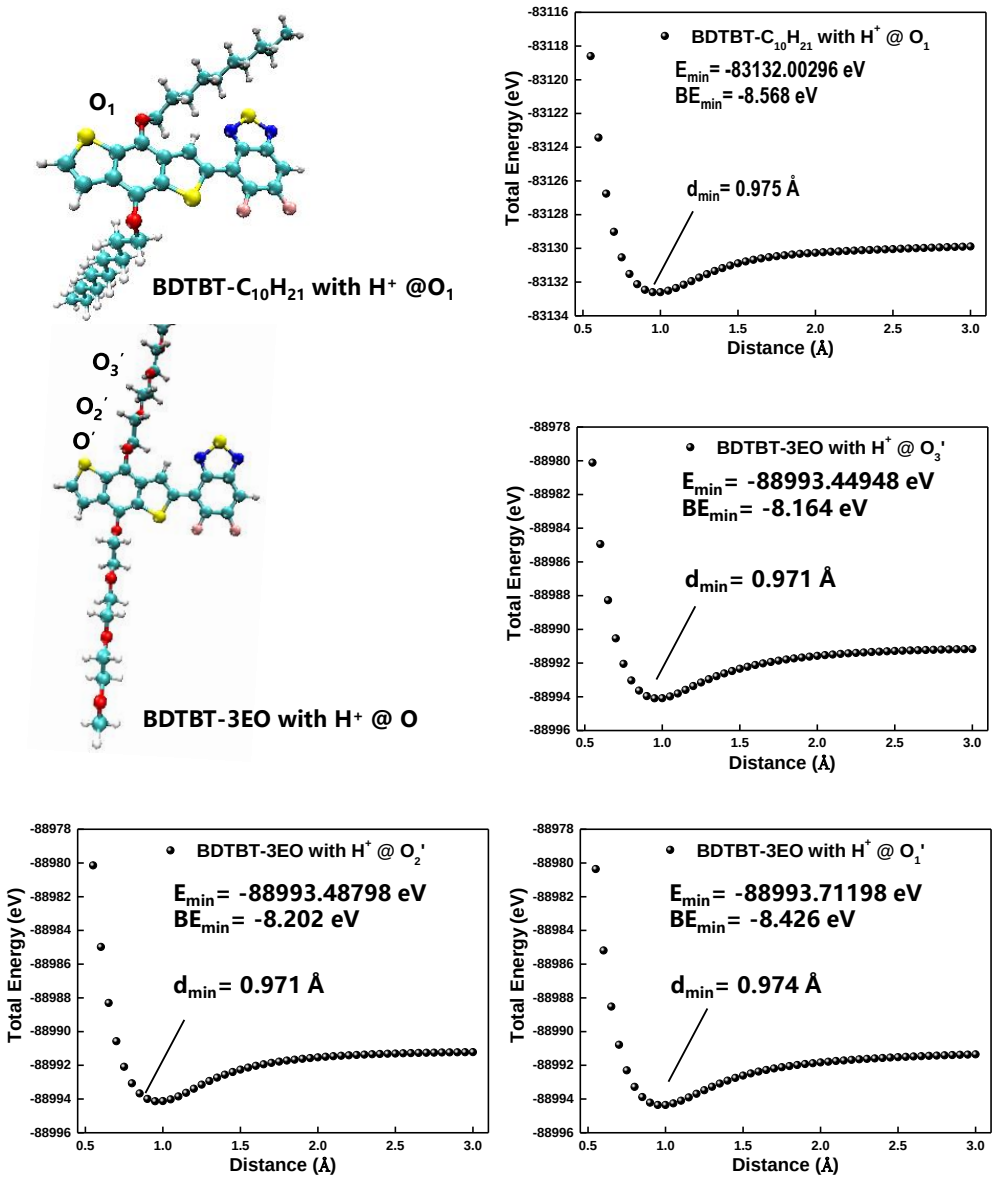

Figure S15. The total energy vs distance plots of BDTBT-$C_{10}H_{21}$ and BDTBT-3EO with one H^+ absorbed in oxygen, related to Figure 5. The minimum contact distances are around 1 Å, and the minimum binding energy can be obtained.

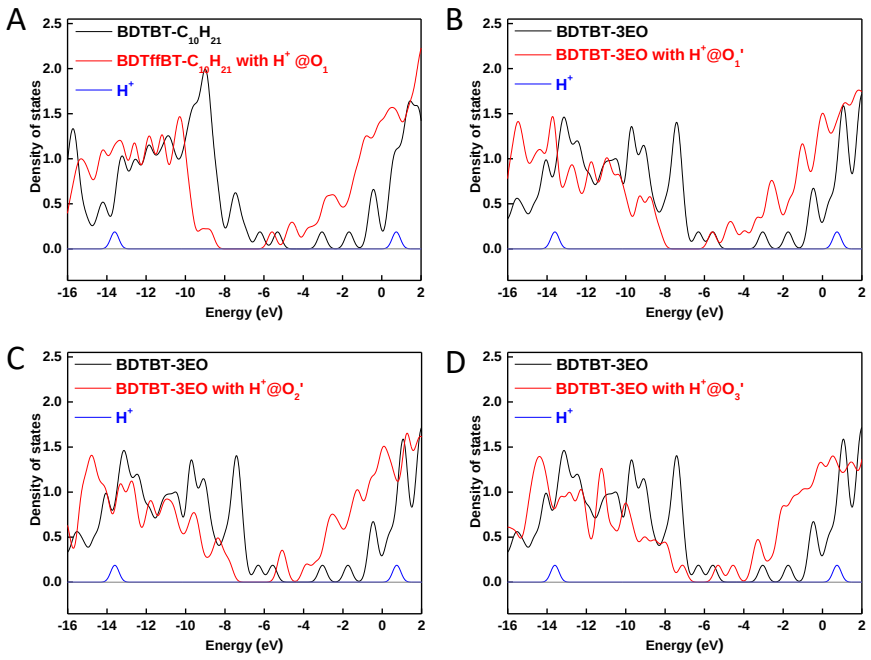

Figure S16. DOS state of BDTBT-$C_{10}H_{21}$ (A) and BDTBT-3EO (B-D) with H^+ absorbed oxygen sites (the case of one hydrogen atom), related to Figure 5.

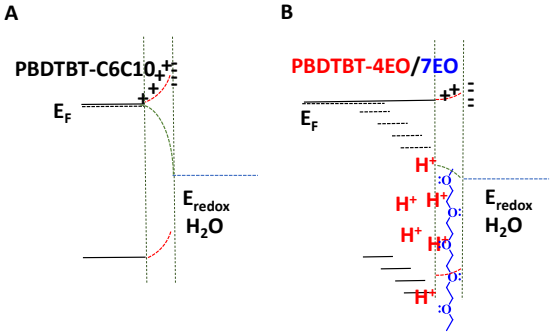

Figure S17. Scheme diagram of energy level changing of (A) PBDTBT-C6C10 and (B) PBDTBT-4EO/7EO in contact with water, related to Figure 5.

Table S1. Performance summary of linear conjugated polymeric photocatalysts, related to Figure 3.

Catalysts	HER (mmol $h^{-1}g^{-1}$)	AQY (wavelength)	Reaction Conditions	Abs. edge	Reference
PPP-11-Ru	0.3		TEA	450	Shibata et al., 1990
PBpy-Py$(bpy)_2$	2.55		H_2O /TEA	420	Maruyama et al., 1997
B-BT-1,4	2.32	4.01% (420 nm)	H_2O /TEOA	517 nm	Yang et al., 2016
Planarized Conjugated Polymer	5.8	2.3 % (420 nm)	H_2O/ CH_3OH /TEA	460 nm	Sprick et al., 2016
PPDI-bpy	0.355	0.02% (525 nm)	H_2O/DEA	600 nm	Li et al., 2016
PT/PVA-Pt		0.06%	MV^{2+}/EDTA	680 nm	Lu et al., 2017
PTh	2.8		AA/H_2O	650 nm	Zong et al., 2017
PFBT Pdots	8.3	0.5% (445 nm)	AA/H_2O	520 nm	Wang et al., 2016
PFODTBT dots (0.1% Pd)	Initial: 50.0 Average: 15.5 (4 h)	0.6% (550 nm)	AA/H_2O	650 nm	Pati et al., 2017
Conjugated copolymer:p8-i	0.86	0.56 % (420nm)	H_2O/CH_3OH /TEA	400 nm	Woods et al., 2017
PFTFQ-PtPy15	10.2 (4 h)	0.40% (515 nm)		610 nm	Tseng et al., 2018
PBDTBT-7EO (3.0 wt% Pt)	15.9	0.30% (600 nm)	AA/H_2O	720 nm	This work

Table S2. Performance summary of part polymeric photocatalysts, related to Figure 3.

Catalysts	HER ($mmolh^{-1}g^{-1}$)	AQY (wavelength)	Reaction Conditions	Abs. edge	Reference
g-C_3N_4 (3.0 wt% Pt)	0.1	0.1 %	H_2O/TEOA	450 nm	Wang et al., 2009
Triazine-based Carbon Nitrides (2.3 wt% Pt)	4.9	3.4%	H_2O/TEOA		Schwinghammer et al., 2013
g-C_3N_4 (3.0 wt% Pt)	15	50.7% (405 nm)	H_2O/TEOA		Lin et al., 2016
g-C_3N_4 (3.0 wt% Pt)	20	26.5%(400 nm)	H_2O/TEOA	450	Martin et al., 2014
g-C_3N_4	23.06	31.07% (420 nm)	H_2O/TEOA		Yu et al., 2018
Conjugated poly(azomethine) (3.0 wt% Pt)	0.07		H_2O/TEOA	510 nm	Schwab et al., 2010
Conjugated copolymer	0.18	4.2%	H_2O/TEOA	650 nm	Sprick et al., 2015
hydrazone-based COF (Pt-modified)	1.9	2.2 % (400 nm)	H_2O/TEOA		Stegbauer et al., 2014
azine hydrazone-based COF (0.68 wt% Pt)	1.5	0.45% (450 nm)	H_2O/TEOA	550 nm	Vyas et al., 2015
Microporous organic nanorods (TiO_2-Pt)	1.25	4.5%	H_2O/TEOA	540 nm	Park et al., 2014
Phenyl-triazine oligomers (2.2 wt% Pt)	0.12	5.5% (400 nm)	H_2O/TEOA		Schwinghammer et al., 2015
Conjugated Polybenzothiadiazoles (3.0 wt% Pt)	2.9	4.0% (420 nm)	H_2O/TEOA	550 nm	Yang et al., 2016
PFBT/C_3N_4 (1% Pt)	0.7	10.1% (500 nm)	H_2O/TEOA	560 nm	Chen et al., 2017
Porous Conjugated Polymers (2.0 wt% Pt)	0.17	1.8% (350 nm)	H_2O/CH_3OH/TEA	620 nm	Li et al., 2016

Transparent Methods

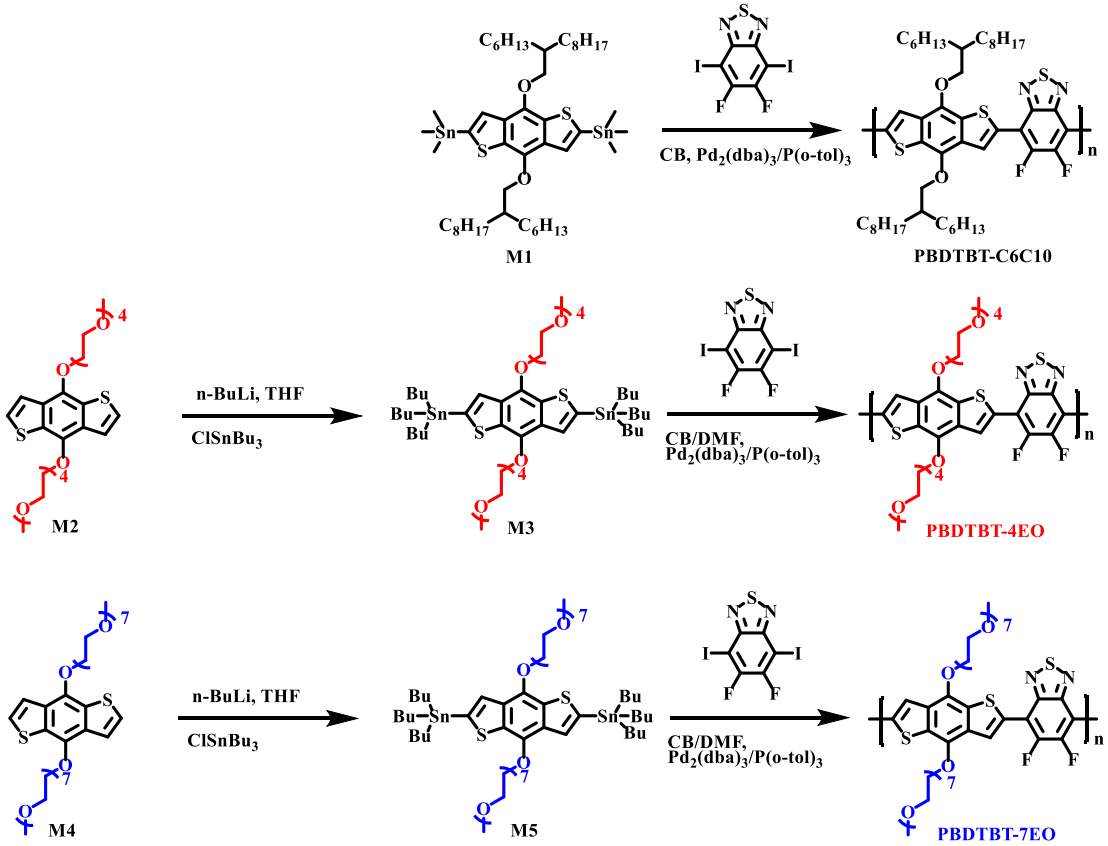

Scheme S1 Synthetic procedures of conjugated polymers, related to Figure 1.

Materials: M1 was purchased from Suna Tech Inc., and used after recrystallization from ethanol. 5,6-difluoro-4,7-diiodobenzo[c][1,2,5]thiadiazole was synthesized according to the published reference (Wang et al., 2013).

PBDTBT-C6C10: PBDTBT-C6C10 was synthesized from M1 and M2 using Stille polymerization in chlorobenzene (CB) in the existence of $Pd_2(dba)_3$ and tri(o-tolyl)phosphine ($P(o\text{-}tol)_3$). M1 (99.8 mg, 0.1 mmol) and 5,6-difluoro-4,7-diiodobenzo[c][1,2,5]thiadiazole (42.4 mg, 0.1 mmol) were placed in a round-bottomed flask, then CB (1.0 mL) was added. The mixture was then degassed for three times to remove the oxygen. Then $Pd_2(dba)_3$ (1.0 mg) and $P(o\text{-}tol)_3$ (2.0 mg) were added, and the mixture was degassed once again and then heated to 140°C for 12 h to get the polymer. The polymer solution was then precipitated into methanol and the solid was collected and dried. Then, the polymer was extracted using Soxhlet extraction from acetone, hexane and chloroform. The chloroform fraction was then concentrated and precipitated into methanol again. The deep blue solid was collected and dried to yield the polymer PBDTBT-C6C10. Yield (73 mg, 87%) ^{1}H-NMR (500MHz, $CDCl_3$, δ ppm): 9.10-7.60 (m, 2H), 4.85-3.15 (m, 6H), 2.50-0.65(m, 60H). GPC (THF), Mn=20.6 kDa, $Đ$=1.21.

M2: M2 was synthesized according to the reported procedure in reference (Nielsen et

al., 2016). ^{1}H-NMR (500MHz, $CDCl_3$, δ ppm):7.58-7.56(d, 2H),7.38-7.37(dd,2H), 4.44-4.42 (m, 4H), 3.88-3.86 (m, 4H), 3.77-3.75 (m, 4H), 3.73-3.69 (m, 4H), 3.68-3.62 (m, 4H), 3.37 (s,6H); ^{13}C-NMR (126MHz, $CDCl_3$, δppm): 144.27, 131.84, 130.29, 126.19, 120.52, 72.81, 71.92, 70.83, 70.68, 70.66, 70.62, 70.56, 70.50, 70.40, 59.01. MS (MALDI-TOF): calcd. for C28H42O10S2, 602.22, found 602.21, 625.19 (MNa^+).

M3: M2 (1.20 g, 2.0mmol) and 20 mL of dry THF was placed in a flask and cooled to-78 °C under the protection of nitrogen. Then, n-BuLi (2 mL, 5.0 mmol, 2.5 M in THF) was slowed added over 10 mins. The reaction was maintained at-78 °C for 1.5 h, then tributylchlorostannane (6 mL, 6.0 mmol, 1.0 M in THF) was added in one portion. The reaction was stirred at-78 °C for 0.5 h and allowed to slowly warm to room temperature overnight. Dichloromethane and water were added, and the organic fraction was collected and washed with water for three times. The organic fraction was concentrated and the crude M3 was purified using a silica gel column chromatography (the silica gel was soaked in trimethylamine and dried before use) with hexane:methanol (15:1 v/v) as eluent. Yield (1.36 g, 58%). ^{1}H-NMR (500MHz, $CDCl_3$, δ ppm): 7.51 (s, 2H), 4.49-4.41 (t, *J* = 5.0 Hz, 4H), 3.93-3.87 (t, *J* = 5.0 Hz, 4H), 3.77 (m, 4H), 3.71-3.61 (m, 16 H), 3.53-3.50 (m, 4H), 3.35 (s, 6H), 1.68-1.54 (m, 12H), 1.41-1.33 (m, 12H), 1.24-1.13 (m, 12H), 0.90 (t, *J* = 7.3 Hz, 18H). ^{13}C NMR (126 MHz, $CDCl_3$, δ ppm): 142.62, 140.27, 134.28, 132.94, 128.12, 72.48, 71.93, 70.84, 70.73, 70.68, 70.61, 70.55, 70.52, 59.02, 28.99, 27.26, 13.70, 10.86. MS (MALDI-TOF): calcd. for C52H94O10S2Sn2, 1180.43 found 1203.39 (MNa^+).

M4： M4 was synthesized using the same procedure to that of M2. ^{1}H-NMR (500MHz, $CDCl_3$, δ ppm): 7.58-7.55(d,2H),7.38-7.36 (dd,2H),4.45-4.40 (m,4H),3.90-3.86 (m,4H),3.78-3.75(m,4H), 3.74-3.61 (m, 40H), 3.56-3.52 (m, 4H), 3.37 (s, 6H); ^{13}C-NMR (126MHz, $CDCl_3$, δppm): 144.27, 131.88, 130.31, 126.23, 120.52, 72.82, 71.91, 70.84, 70.67, 70.60, 70.57, 70.54, 70.48, 70.43, 59.02. MS (MALDI-TOF): calcd. for C40H66O16S2, 866.38, found 866.34.

M5: M5 was synthesized using the same procedure to that of M3. Yield(1.76 g, 61%) ^{1}H-NMR (500MHz, $CDCl_3$, δ ppm): 7.51 (s,2H),4.47-4.45(m,4H),3.91-3.89(m,4H),3.72-3.71(m,4H), 3.69-3.62(m,36H), 3.55-3.53 (m,4H), 3.37(s,6H), 1.65-1.58 (m, 12H), 1.39-1.33 (m, 12H), 1.20-1.17 (m, 12H), 0.91 (t, *J* = 7.3 Hz, 18H). MS (MALDI-TOF): calcd. for C64H118O16S2Sn2, 1444.59, found 1444.54, 1467.53 (MNa^+).

PBDTBT-4EO: M3 (118.1 mg, 0.1 mmol) and 5,6-difluoro-4,7-diiodobenzo[c][1,2,5]thiadiazole (42.4 mg, 0.1 mmol) were placed were placed in a round-bottomed flask, then CB (0.5 mL) and DMF (0.5 mL) were added. The mixture was then degassed for three times to remove the oxygen. Then $Pd_2(dba)_3$ (1.0 mg) and $P(o\text{-}tol)_3$ (2.0 mg) were added, and the mixture was degassed once again and then heated to 140°C for 12 h to get the polymer. The polymer solution was then precipitated into acetone and the solid was collected and dried. Then, the polymer was extracted using Soxhlet extraction from acetone, hexane, and chloroform. The chloroform fraction was then concentrated and precipitated into acetone again. The deep blue solid

was collected and dried to yield the polymer PBDTBT-4EO. Yield (70 mg, 91%) ^{1}H-NMR (500MHz, $CDCl_3$, δ ppm): 8.70-7.60 (m, 2H), 4.90-3.10 (m, 38H). GPC (THF), Mn=26.5kDa, *Đ*=1.57.

PBDTBT-7EO: PBDTBT-7EO was synthesized using the same procedure with that of PBDTBT-4EO. Yield (89 mg, 86%) ^{1}H-NMR (500MHz, $CDCl_3$, δ ppm): 8.75-7.80 (m, 2H),4.85-3.25 (m,38H). GPC (THF), Mn=29.6kDa, Đ=3.85.

Characterization: ^{1}H NMR and ^{13}C NMR spectra of the monomers and polymers were recorded on a Bruker AV-600 spectrometer with $CDCl_3$ as solvent. Molecular weights of polymers were determined by a Waters GPC 2410 with a refractive index (RI) detector and using a calibration curve with polystyrene standards where THF was used as mobile phase. UV-vis spectra of the polymers were collected on a HP 8453 spectrophotometer. For the solution absorption, the polymers were dissolved into $CHCl_3$ with a concentration of 0.02 mg mL^{-1}. Samples for film absorption of these polymers were prepared by spin-coating their solutions (10 mg mL^{-1}) into quartz glasses. Photoluminescence (PL) spectra were measured using a Jobin-Yvon spectrofluorometer. Cyclic Voltammetry (CV) measurements were conducted in a CHI660E elctrochemical work-stastation where a glassy carbon electrode was used as working electrode. An Ag/AgCl electrode was used as reference electrode and a Pt wire was used as counter electrode. The measurements were conducted in anhydrous acetontrile with tetrabutylammonium hexafluorophosphate (Bu_4NPF_6, 0.1 M) as supporting electrolyte under argon atmosphere. The scan rate is 0.05 V/s. The potential of the Ag/AgCl electrode was calibrated using the ferrocene/ferrocenium (Fc/Fc^{+}), which delivered a reduction potential of -4.8 eV. X-ray photoelectronic spectroscopy (XPS) was measured on a Thermo Electron ESCALAB 250 spectrometer equipped with a monochromatic Al X-ray source (1486.6 eV). Water contact angle measurements were performed on a VCA15 surface contact angle analyzer (Dataphysics). UPS measurements were performed on the Thermo ESCALAB 250XI. The Valance band (*VB)* spectra were measured with a monochromatic He I light source (21.2 eV) and a VG Scienta R4000 analyzer. A sample bias of-5 V was applied to observe the secondary electron cutoff. The FT-IR spectra of these polymers were obtained from VERTEX 70(Bruker). X-ray powder diffraction of these polymers in powder state was performed on Bruker D8 ADVANCE. The high resolution transmission electron microscope (HR-TEM) images of the dispersed polmers was obtained from TF20, Joel 2100F Microscope.

Electrochemical Analysis. The electrochemical experiments were conducted with a CHI660E Electrochemical System in a three electrode cell with a Pt sheet as the counter electrode and an Ag/AgCl electrode (3 M KCl) as the reference electrode. The working electrodes were prepared by coating polymers (10 mg mL^{-1} in $CHCl_3$) onto ITO glasses with thicknesses about 300 nm. The active area is confined to 0.50 cm^2. A 0.1 M Na_2SO_4 aqueous solution (pH = 6.8) was chosen as the supporting electrolyte and was purged with nitrogen for 30 min to remove O_2 before any measurements. The working electrodes for photocurrent test were illuminated with a solar simulator (300-W Xe light source, λ > 300 nm). For Mott-Schottky plots, the E_{FB} was extracted from Mott-Schottky

equation: $\frac{1}{C^2} = \frac{2(E-E_{FB}-k_B\mathrm{T/e})}{\varepsilon\varepsilon_0 \mathrm{A}^2 e N_D}$. According to this Equation, a straight tangent line can be drawn by using a plot of $1/C^2$ vs E, and E_{FB} can be determined by the intercept of the straight line with E axis.

Photocatalytic hydrogen evolution: The hydrogen evolution measurements were performed on a Labsolar-IIIAG photocatalytic system (PerfectLight) equipped with a 50-mL reactor. For the photocatalytic experiment, polymers (2.5 mg) were firstly dissolved in 250 μL of THF and then dispersed into a mixture of 50 mL of AA solution (0.2 M, pH = 4.0 adjusted by NaOH aq.). The total concentration of the polymers for photocatalytic measurement in reaction solution was 50 μg/mL. The reaction was held in a vacuum for 30 min to remove the dissolved oxygen and THF, followed by ultrasonication for 1 h. The photocatalytic experiments were then degassed again and illuminated with a solar simulator (300-W Xe light source, λ > 300 nm). Pt co-catalysts were prepared by dissolving H_2PtCl_4 into the polymer solution with irradiation for 1 h, which enables the formation of Pt nanoparticles (Chen et al., 2017). The calculated weight of Pt co-catalysts is 3% of that of each polymer. The luminous power reaching the surface of the reaction solution was calibrated to be 162.4 mW cm^{-2} by a power meter. The produced gas was analysed by a GC7900 gas chromatograph. Hydrogen was detected with a thermal conductivity detector, referencing against standard gas with a known concentration of hydrogen. The AQY was measured at selected wavelengths enabled by different band pass filters (CELQD, 380, 420, 450, 550, 600, 650 and 700 nm). The AQY at a given wavelength was calculated from the following equations:

$N_o=(E\lambda T\%)/hc$; $N=(V\times 6.02\times 10^{23})/(22.4t)$;$AQY=2N/No$

N_o represents the number of incident photons, N represents the number of collected H_2 molecules, E represents the energy of incident light at a given wavelength, determined by a calibrated power meter, λ represents the wavelength of incident light, V represents the volume of H_2 molecules detected in a fixed time (t), determined by GC, T% represents the transmittance of the quartz cell.

References:

Maruyama, T., and Yamamoto, T. (1997). Effective photocatalytic system based on chelating π-conjugated poly(2,2′-bipyridine-5,5′-diyl) and platinum for photoevolution of H_2 from aqueous media and spectroscopic analysis of the catalyst. *J. Phys. Chem. B* 101, 3806.

Yang, C., Ma, B. C., Zhang, L., Lin, S., Ghasimi, S., Landfester, K., Zhang, K. A. I., and Wang, X. (2016) Molecular engineering of conjugated polybenzothiadiazoles for enhanced hydrogen production by photosynthesis. *Angew. Chem. Int. Ed*. 55, 9202.

Sprick, R. S., Bonillo, B., Clowes, R., Guiglion, P., Brownbill, N. J., Slater, B. J., Blanc, F., Zwijnenburg, M. A., Adams, D. J., and Cooper, A. I. (2016). Visible-light-driven hydrogen evolution using planarized conjugated polymer photocatalysts. *Angew. Chem. Int. Ed*. 55, 1792.

Li, L., Hadt, R. G.,Yao, S., Lo, W.-Y., Cai, Z., Wu, Q., Pandit, B., Chen, L.-X., and Yu, L. (2016). Photocatalysts based on cobalt-chelating conjugated polymers for hydrogen evolution from water. *Chem. Mater.* 28, 5394.

Lu, H., Hu, R., Bai, H., Chen, H., Lv, F., Liu, L., Wang, S., and Tian, H. (2017). Efficient Conjugated polymer–methyl viologen electron transfer system for controlled photo-driven hydrogen evolution. *ACS Appl. Mater. Interfaces 9*, 10355.

Zong, X., Miao, X., Hua, S., An, L., Gao, X., Jiang, W., Qu, D., Zhou, Z., Liu, X.and Sun, L. (2017). Structure defects assisted photocatalytic H_2 production for polythiophene nanofibers. *Appl. Catal. B-Environ.* 211, 98.

Wang, L., Fernández-Terán, R., Zhang, L., Fernandes, D. L., Tian, L., Chen, H., and Tian, H. (2016). Organic polymer dots as photocatalysts for visible light-driven hydrogen generation. *Angew. Chem. Int. Ed*. 55, 12306.

Pati, P. B., Damas, G., Tian, L., Fernandes, D. L. A., Zhang, L., Pehlivan, I. B., Edvinsson, T., Araujo, C. M., and Tian, H. (2017). An experimental and theoretical study of an efficient polymer nano-photocatalyst for hydrogen evolution. *Energy Environ. Sci*. 10, 1372.

Woods, D. J., Sprick, R. S., Smith, C. L., Cowan, A. J., and Cooper, A. I. (2017). A solution-processable polymer photocatalyst for hydrogen evolution from water. *Adv. Energy Mater.* 7, 1700479.

Tseng, P.-J., Chang, C.-L., Chan, Y.-H., Ting, L.-Y., Chen, P.-Y., Liao, C.-H., Tsai, M.-Li and Chou, H.-H. (2018) Design and synthesis of cycloplatinated polymer dots as photocatalysts for visible-light-driven hydrogen evolution. *ACS Catal*. 8, 7766.

Wang, X., Maeda, K., Thomas, A., Takanabe, K., Xin, G., Carlsson, J. M., Domen, K., and Antonietti, M. (2009). A metal-free polymeric photocatalyst for hydrogen production from water under visible light. *Nat. Mater.* 8, 76.

Schwinghammer, K., Tuffy, B., Mesch, M. B., Wirnhier, E., Martineau, C., Taulelle, F., Schnick, W., Senker, J., and Lotsch, B. V. (2013). Triazine-based carbon nitrides for visible-light-driven hydrogen evolution. *Angew. Chem. Int. Ed*. 52, 2435.

Lin, L., Ou, H., Zhang, Y., and Wang, X. (2016). Tri-s-triazine-based crystalline graphitic carbon nitrides for highly efficient hydrogen evolution photocatalysis. *ACS Catal*. 6, 3921.

Martin, D. J., Qiu, K., Shevlin, S. A., Handoko, A. D., Chen, X., Guo, Z., and Tang, J. (2014). Highly efficient photocatalytic H_2 evolution from water using visible light and structure-controlled graphitic carbon nitride. *Angew. Chem. Int. Ed.* 53, 9240.

Yu, Y., Yan, W., Wang, X., Li, P., Gao, W., Zou, H., Wu, S., and Ding, K. (2018). Surface engineering for extremely enhanced charge separation and photocatalytic hydrogen evolution on g-C_3N_4. *Adv. Mater.* 30, 1705060.

Schwab, M. G., Hamburger, M., Feng, X., Shu, J., Spiess, H. W., Wang, X., Antonietti, M., and Müllen,

K. (2010). Photocatalytic hydrogen evolution through fully conjugated poly(azomethine). networks. *Chem. Commun*. 46, 8932.

Sprick, R. S., Jiang, J. –X.,Bonillo, B., Ren, S., Ratvijitvech,T., Guiglion,P., Zwijnenburg, M. A., Adams, D. J., and Cooper, A. I. (2015). Tunable organic photocatalysts for visible-light-driven hydrogen evolution. *J. Am. Chem. Soc.* 137, 3265.

Stegbauer, L., Schwinghammer, K., and Lotsch, B. V. (2014). A hydrazone-based covalent organic framework for photocatalytic hydrogen production. *Chem. Sci.* 5, 2789.

Vyas, V., Haase, F., Stegbauer, L., Savasci, G., Podjaski, F., Ochsenfeld, C., and Lotsch, B. V. (2015). A tunable azine covalent organic framework platform for visible light-induced hydrogen generation. *Nat. Commun*. 6, 8508.

Park, J. H., Ko, K. C., Park, N., Shin, H.–W., Kim, E., Kang, N., Ko, J. H., Lee, S. M., Kim, H. J., Ahn, T. K., Lee, J. Y., and Son, S. U. (2014). Microporous organic nanorods with electronic push–pull skeletons for visible light-induced hydrogen evolution from water. *J. Mater. Chem. A* 2, 7656.

Schwinghammer, K., Hug, S., Mesch, M. B., Senker, J., and Lotsch, B. V. (2015). Phenyl-triazine oligomers for light-driven hydrogen evolution. *Energy Environ. Sci*. 8, 3345.

Yang, C., Ma, B. C., Zhang, L., Lin, S., Ghasimi, S., Landfester, K., Zhang, K. A. I., and Wang, X. (2016). Molecular engineering of conjugated polybenzothiadiazoles for enhanced hydrogen production by photosynthesis. *Angew. Chem. Int. Ed*. 128, 9202.

Li, L., Cai, Z., Wu, Q., Lo, W-Y., Zhang, N., Chen, L. X., and Yu, L. (2016). Rational design of porous conjugated polymers and roles of residual palladium for photocatalytic hydrogen production. *J. Am. Chem. Soc*. 138, 7681.

Wang, N., Chen, Z., Wei, W., and Jiang, Z. (2013). Fluorinated benzothiadiazole-based conjugated polymers for high-performance polymer solar cells without any processing additives or post-treatments. *J. Am. Chem. Soc*. 135, 17060

Nielsen, C. B., Giovannitti, A., Sbircea, D.T., Bandiello, E., Niazi, M. R., Hanifi, D. A., Sessolo, M., Amassian, A., Malliaras, G., Rivnay, J., and McCulloch. I. (2016). Molecular design of semiconducting polymers for high-performance organic electrochemical transistors. *J. Am. Chem. Soc.* 138, 10252.

Chen, J., Dong, C.-L., Zhao, D., Huang, Y.-C., Wang, X., Samad, L., Dang, L., Shearer, M., Shen, S., and Guo, L. (2017). Molecular design of polymer heterojunctions for efficient solar–hydrogen conversion. *Adv. Mater.* 29, 1606198.

Shibata, T., Kabumoto, A., Shiragami, T., Ishitani, O., Pac, C., and Yanagida, S. (1990). Novel visible-light-driven photocatalyst. poly(p-phenylene)-catalyzed photoreductions of water, carbonyl compounds, and olefins. *J. Phys. Chem*. 94, 2068.